NAZARBAYEV UNIVERSITY

School of Engineering and Digital Sciences

Bachelor of Engineering in
Mechanical and Aerospace Engineering

Employing 2D material in reinforcing interface strength in fiber-reinforced metal laminates

(Final Capstone Project Report)

by

Azamat Malgazhdar, Zhussip Sagitkhan,
and Assel Nemerenova

Lead Supervisor: Prof. Sherif Gouda
Co-Supervisor: Prof. Gulnur Kalimuldina
April, 2024

Declaration

We, Azamat Malgazhdar, Zhussip Sagitkhan, and Assel Nemerenova, hereby declare that this report, entitled “Employing 2D material in reinforcing interface strength in fiber - reinforced metal laminates” is the result of our own project work except for quotations and citations which have been duly acknowledged. We also declare that it has not been previously or concurrently submitted for any other degree at Nazarbayev University or elsewhere.

_____

Name: Azamat Malgazhdar

_____

Name: Zhussip Sagitkhan

_____

Name: Assel Nemerenova

Date: April 28, 2024

Acknowledgment

We take this opportunity to express our gratitude to our supervisor professor Sherif Gouda and co-supervisor professor Gulnur Kalimuldina for their active support, guidance and valuable advice.

We are highly thankful to Dr. Umut Backbergen for her active mentorship throughout the project and invaluable support. Her expertise and generosity have played an important role throughout our capstone project.

We also would like to express our special thanks to the research team for the guidance in the laboratory and Nazarbayev University for providing us with the necessary resources and equipment.

Abstract

This study was conducted with the aim of improving fiber-metal laminates (FMLs) by strengthening the interface between layers using 2D materials such as the α-Zirconium phosphate (α-ZrP). The importance of this topic is emphasized by an analysis of the literature, which reveals a gap in research in the field of application of α-ZrP nanomaterials. Even though α-ZrP was discovered and synthesized a long time ago, there is a lack of studies in using it as a reinforcement for fiber metal laminates. To achieve this goal a research were conducted to synthesize and characterize α-ZrP nanoparticles. Then some experiments were performed to find the best composition of the polymer starting from 0 wt% to 2 wt% of these nanoparticles by using the commercial polyurethane. Several single lap joint samples using the aluminum sheets were made and additionally pure polyurethane polymers were examined for the extra information about the adhesive layer. Mechanical and electrochemical treatments were implemented for the improvement of the interlocking mechanism between the metal and adhesive polymer. In addition, the synergetic effect of their combination with nanoparticles was studied. The behavior of the composite was studied using different testing types such as the single lap shear strength test and tensile strength test for pure polyurethane as well as it was analyzed by the Finite Element Analysis (FEA) using the ABAQUS software. Ultimate tensile strengths were determined for the comparison of the experimental and numerical parts' results and the best concentration for the pure polymer was found to be 1.0 wt% of α-ZrP with 3.5 times enhanced tensile strength, while for single lap joints it was 0.5 wt% which increased the shear strength by 91.8%. Mechanical treatment by itself significantly increases the shear strength of lap joints by 35%, although it reduces efficiency in combination with nanoparticles. Conversely, electrochemical treatment, especially combined with nano reinforcement showed superior performance in terms of increase of the shear strength by 174% compared to all other treatments. Although the combination of nanoparticles with both treatments provided a slight increase in strength by 18.9%, this did not correspond to the significant increase achieved by electrochemical treatment. The initial hypothesis was proved and supported with numerical modeling.

Contents

List of Figures

Chapter 1

Introduction

Advanced materials have become one of the most compelling research areas since the 1980s, gaining increasing attention in recent years from both the scientific and industrial communities. This significant rise of interest in advanced materials stems from their unique properties, often referred to as 'smart' or 'intelligent,' which can be manipulated to suit specific applications. For researchers aiming to develop these types of materials with improved multifunctionality, durability, and customization, it's crucial to carefully consider their microstructure and composition. By controlling these factors, there is potential to create the next generation of materials with enhanced reliability and efficiency [1]. There are a lot of different types of smart materials, however, one subset that are of primary importance for this project is composites materials. Their exceptional abilities of structural integrity and unmatched level of customization through material blending distinguish them from other intelligent materials.

Composite materials are formed by combining two or more different materials, with one acting as the matrix, while the second as a phase is dispersed within the first. This combination results in a material that inherits the properties of each individual component, creating a composite with superior characteristics compared to the original materials. While the dispersed phase may take the form of particles, flakes, in significant examples, it is in the form of fibers. Consequently, fiber composites become one of the most promising subdivisions within this class of engineering materials for many industrial sectors [2].

Nowadays, due to the environmental situation worldwide, the European Commission is setting environmental, safety, and fuel efficiency standards for advanced transportation technology [3]. This, in turn, pushes the technological industries, such as aerospace and automotive, to develop and utilize more composite materials in the design and manufacturing of structural components. As per Trzepieciński et al.'s analysis, for example, each Boeing 787 aircraft has over 32,000 kg of carbon fiber-reinforced polymer (CFRP) composites, which make up almost 80% of the aircraft's volume by composites (Figure 1.1) [4]. However, not all critical structural components, like the fuselage, can be fabricated from single-fiber composites, as they require improved fatigue resistance, higher damage tolerance, and better thermal

stability, given their role in passenger safety and the mitigation of catastrophic failures. Therefore, one way to address two major concerns related to high weight and fatigue strength is the utilization of a combined material consisting of lightweight metal and fiber-reinforced polymer composites. The use of aluminum, which has a density of about 2.7 g/cm³, provides a 30–50% weight reduction [3]. However, because aluminum (Al) is susceptible to fatigue stress, strategies for prolonging its fatigue life without sacrificing its lightweight and workability have been developed. Fiber metal laminates (FMLs), in particular, have produced some of the most successful and affordable components when aluminum is used in composites. That is why, in the context of fiber composites, the current industry emphasis is on the investigation of Fiber Metal Laminates (FMLs).

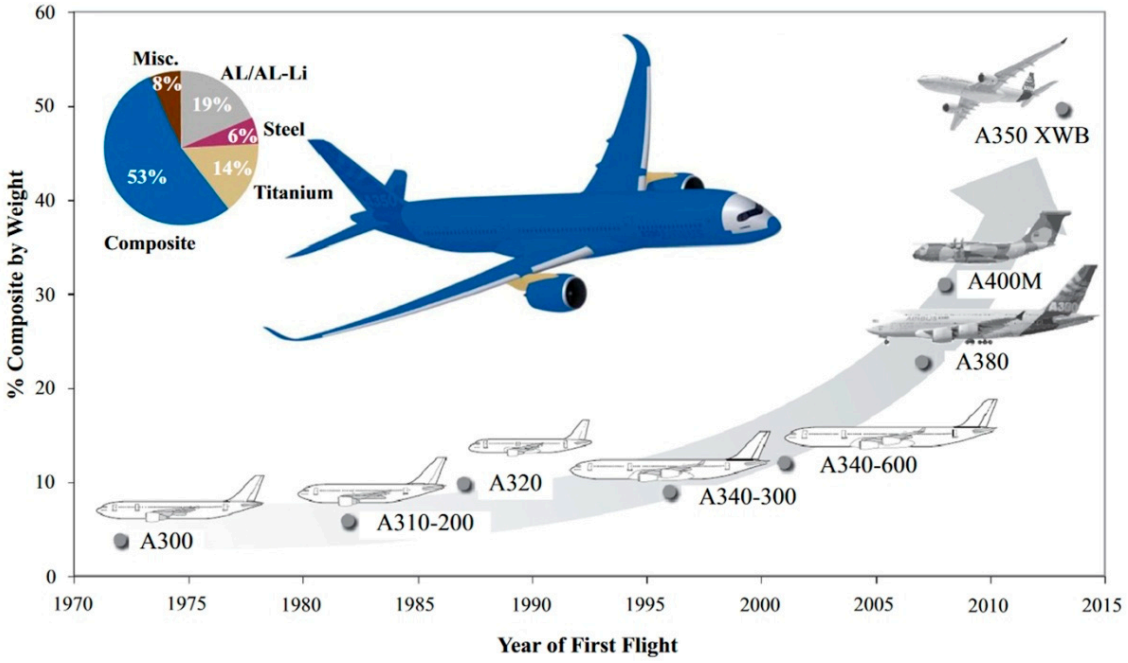

Figure 1.1. Use of composite materials in Airbus aircraft [4]

The structural materials known as FMLs is a specific class of composite materials that combine metal layers with fibers and provide special benefits in terms of strength, flexibility, and customized functions. FMLs stand out for having excellent stiffness-to-weight and strength-to-weight ratios. They have exceptional resistance to corrosion and moisture, great fracture toughness, outstanding fatigue resistance, and excellent impact strength. These materials are hybrid composites made of layers of fiber-reinforced polymers and thin metal sheets [5]. The qualities and failure characteristics of these materials can be customized based on the type of metal, fiber,

and polymer. The general structure of FMLs is illustrated in Figure 1.2 and the most widely available FMLs, according to Tamer et.al., are CARALL (Carbon Reinforced Aluminium Laminate), GLARE (Glass Reinforced Aluminium Laminate), and ARALL (Aramid Reinforced Aluminium Laminate) [5].

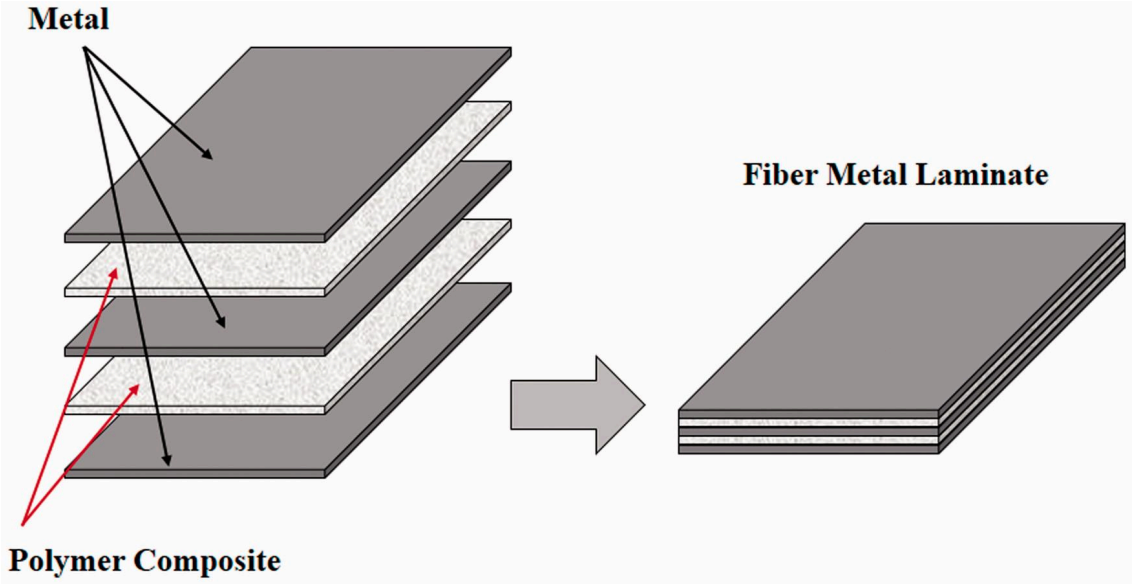

Figure 1.2. Schematic presentation of fiber metal laminate [6]

It is determined that the primary factor influencing the total mechanical performance and service life of an FMLs component is the interface strength (bonding) between laminates, fiber, and matrix. Recognizing this, researchers acknowledged the necessity for nanoparticle reinforcement, through the incorporation of nanomaterials and application of surface treatment in Fiber Metal Laminates (FMLs). Such reinforcement or treatment procedures are anticipated not only to enhance interface bonding strength but also to facilitate tailorable properties based on specific applications. An illustrative example of nanomaterial utilization in FMLs can be found in the research by Wang et al. In this study, graphene nanoplatelets (GnPs) were incorporated to enhance the mechanical properties of FMLs. The results indicate higher impact strength, flexural strength, and flexural modulus for FMLs with nanoparticles compared to those without [7]. Similarly, another research paper highlights that metal surface treatment provides higher adhesion between layers and increases free surface energy in the FMLs [8]. So, these studies provide valuable information about the impact of various interface strengthening techniques on the mechanical performance of FMLs.

In this research project, the focus is on α-Zirconium phosphate (α-ZrP) nanoparticles to strengthen polymers and the interface between the layers. The crystalline form of α-ZrP nanomaterial was initially synthesized in 1964, and since then, these nanoparticles have been widely applied across various fields due to their versatile and commendable characteristics [9]. One of the notable features of the α-ZrP is that it has quite good thermal stability properties, which are of utmost importance in aerospace or automotive industries.

After conducting a thorough review of the existing literature on FMLs, it is evident that a significant research gap exists with regard to the application of α-ZrP nanomaterials in FMLs, which shows the novelty of the given research. FMLs are in common use in major spheres like plane construction and building the bodywork for vehicles. Thus, this identified gap underscores the critical significance of our research topic.

Due to the complex structure and the need for specific equipment setups in FMLs fabrication, the study will be conducted using single-lap joint specimens. We use them because they enable us to predict trends in the data from FMLs, ensuring that our findings from the simpler single-lap joints (SLJ) are applicable to the more complex structures like FMLs.

The main aims and objectives of the research project are the following

Aim: To address existing issues in FMLs by utilizing the special qualities of 2D materials, improving these advanced composites as reinforcements for enhancing interface strength.

Objectives:

- Investigate the effect of α-Zirconium phosphate (α-ZrP) nanoparticles by using 0–2 wt% concentrations in polyurethane Al alloy laminates through experimental testing and finite element analysis (FEA)
- Analyze the effects of mechanical roughening and electrochemical surface treatments on single lap joints through mechanical testing
- Identify Young modulus, Ultimate tensile strength, strain at break values and damage models

Hypothesis: Incorporation of α - ZrP nanoparticles and application of surface treatment improve the interlaminar strength in single-lap joints.

The task distribution for the research project inside the team, was according to the following table.

Table 1.1 The task distribution for the research project

Student Names	Task Distribution
Azamat Malgazhdar	**Experimental Part:** ● Preparation of single-lap joint specimens and polyurethane samples ● Testing of single-lap joint specimens ● Mechanical treatment of specimens
Assel Nemerenova	**Experimental Part:** ● Preparation of single-lap joint specimens and polyurethane samples ● Testing of polyurethane samples ● Electrochemical treatment of specimens
Zhussip Sagitkhan	**Numerical Part:** ● Setup of Simulations ● Numerical Modeling ● Numerical Calculations

Chapter 2

Literature review

2.1 Nanomaterials in FMLs

In recent years there has been a paradigm shift in the search for the new materials that will be able to provide improved mechanical qualities, including lighter weight, and increased durability in the aerospace and automotive industries. In order to increase the mechanical properties, different types of reinforcement (Figure 2.1) can be implemented and one of the most popular products of such enhancement results is considered to be fiber metal laminates that are reinforced by incorporation of fibers into its matrix structure [10].

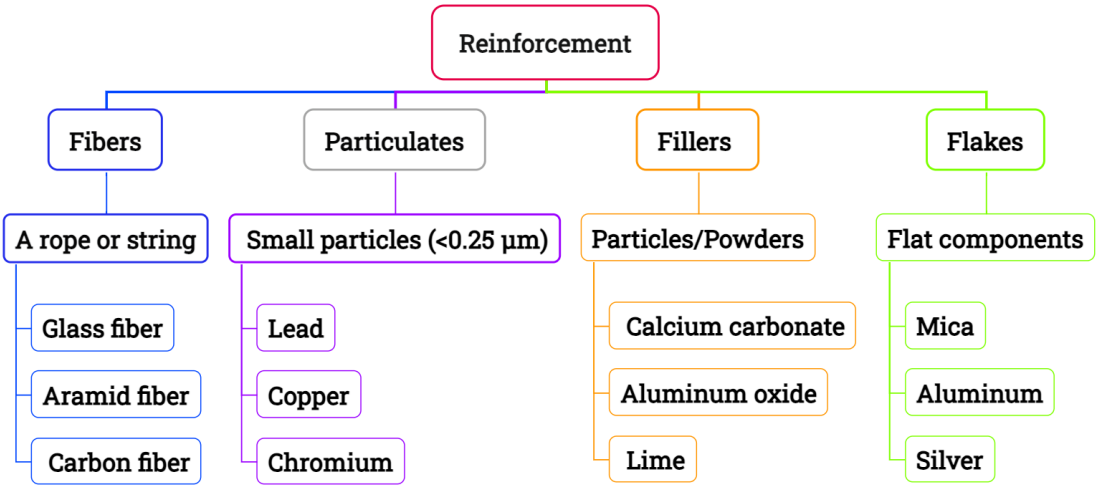

Figure 2.1. The types of reinforcement

Fiber metal laminates (FMLs) are a potential new class of hybrid materials that combine the best features of metal and fiber-reinforced composite materials that have remarkable strength-to-weight and stiffness-to-weight ratios [5, 11-12]. As it was mentioned above, they are widely used in the aerospace industry because of their remarkable wear resistance and excellent damage tolerance [13-16].

Although FMLs have better mechanical properties than other monolithic structural materials, such as aluminum alloys, under quasi-static, dynamic and shock loads, their use for military and commercial purposes is less common than that of conventional composites and metal alloys because there is still a problem of failure

issues. The main reason for fiber metal laminates failure is unpredictable and complex. However, interlaminar and intralaminar failures are often the two main types of damage. Typical FMLs defects include matrix cracking, delamination and degumming between the metal layer and the matrix material [17-22]. Delamination is one of the most common forms of failure and could be caused by relatively weak interlaminar strengths, high shear stress in the component and excessive peel stresses [23]. Wang et al. [7] demonstrated that when a shock load is applied, laminates reinforced with carbon fiber from epoxy resin/aluminum alloy are damaged as a result of delamination, fiber rupture and metal destruction. Similar results were obtained in the study of Al-Azzawi et al. [24], in which laminates made of fiberglass, epoxy resin and aluminum alloy were studied during a 4-point bending test. Therefore, there is a high need for the further improvement of the structure which could be reached with the help of the reinforcement with the particulates as in Figure 2.1. Particle reinforcement is usually used due to low cost and ease of production and forming [10]. This is the best type of the enhancement which is useful when dealing with the delamination issues due to cracks. As it is seen in Figure 2.2 nanoparticles can block the way of the propagation of the crack and stop it, preventing the failure.

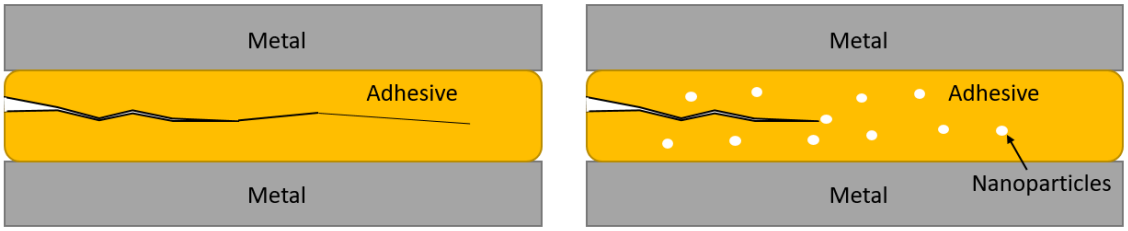

Figure 2.2. Nanoparticles preventing crack propagation in composite materials

Several researchers tried to accomplish this new method to get better results and they used different nanoparticles. For example, Megahed et al. [25] enhanced the mechanical characteristics of GLARE laminates by incorporating 1 wt% nanofillers, which included Al, Cu, TiO2, SiO2, Al2O3, and nanoclay, into the resin matrix of GLARE laminates. Apart from that, multi-walled carbon nanotubes (MWCNT) were studied by Aghamohammadi et al. [26] in connection with their influence on the bending and high-speed impact characteristics of FMLs. They concluded that there was a significant improvement in bending characteristics due to the effective connection of MWCNT in the FMLs structure. In particular, the flexural strength and modulus of elasticity of FMLs increased by 36.62% and 60.16% correspondingly, when 0.5 wt%

MWCNTs was added. However, as it turned out, the inclusion of MWCNT has a negative impact on the characteristics of a high-speed impact. Askin and Touren [27], in turn, used graphene platelets (GnPs) and found that the addition of 1 wt% of GnP increased the interlayer shear strength by 24% and the tensile strength by 9%. Moreover, the constant compressive strength of the composite material has increased by about 50%. Zarei et al. [28] added nylon 6.6 nanofibre non-woven mats between the aluminum plate and fiberglass prepreg. Even though they found no significant effect on the dynamic impact response of GLARE, the bonding strength of the composite was increased.

Several tests were performed to evaluate the FMLs strengthened with the nanoparticles. Wang et al. [7] tested their samples under quasi-static loading (three-point flexure) and dynamic loading (Charpy impact). Khurram et al. [22] evaluated the performance of mechanical properties of FMLs enhanced with the carbon nanotubes with the help of the single lap shear strength test and tensile test that were conducted to evaluate the changes in the interlaminar strength and strength of pure polymer material with presence of nanomaterials. After a number of tests, authors identified the highest value was shown with the 2.0% of the weight percentage of MWNCT. Furthermore, based on the results researchers suggest that increased weight percentage of carbon nanotubes significantly improved the strength of the composite structure.

α-ZrP is an inorganic layered compound that is used in many fields due to its extraordinary characteristics [29]. It has been used as a filler for the creation of polymer nanocomposites, which, compared with a pure polymer, had better physico-chemical characteristics [30]. This nanoparticle is quite unique due to its wide range of applications, flame retardancy, anti-corrosive characteristics and it is even biocompatible [29]. Despite the fact that there are many research papers on a topic of reinforcement of fiber metal laminates with nanoparticles and the method of introducing α-ZrP is not new, there is still a lack of studies about the enhancement with this nanoparticle. Moreover these nanoparticles were mainly used before as reinforcement for the polymer but not for the fiber metal laminates [31], which opened the way for new research and discoveries. That is why, the α-ZrP is used as a nanomaterial for reinforcement of the composite material for our research.

Apart from particulate reinforcement there are also other factors such as surface treatment that can affect the interlaminar strength of the fiber metal laminates. The surface treatment of metals can lead to the optimizing the adhesion between the faces through increase of active chemical groups. Various methods have been used by several researchers: chemical etching, mechanical, anodizing, etc [32].

Mechanical treatment creates greater surface area and improves the mechanical interlocking between the metal and the adhesive [32]. Mohammad et al. [33] investigated the effect of mechanical abrasion on the mechanical properties of carbon fiber aluminum laminates. They found out that the surface made by the sandpaper of the highest roughness showed better strength results.

The electrochemical and chemical treatments change the chemical nature of the metal. The better adhesion is formed due to the porous nanostructure of the oxide surface layer created by this method and where the polymer can penetrate [32]. For example, Arrowsmith and Clifford [34] used anodizing based on sulfuric acid and on phosphoric acid. They studied the surface morphology and found out that sulfuric acid anodizing formed an anodic oxide layer on a metal surface with pore diameter of about 23.5 nm, while phosphoric acid anodizing produced even wider pores. Moreover, Ahmad Marzuki et al. [35] reported that the strength of the FML after phosphoric acid anodizing can increase up to 26% when compared to the reference sample without any treatment. In a research of Fiore et al. [36] anodizing by tartaric sulfuric acid solution gave an increase in mechanical strength up to 130% in comparison to the reference samples .

Aghamohammadi et al. [32] conducted a study where they investigated the effect of different surface treatment on a mechanical strength of the FML. They concluded that Forest Products Laboratory etching (FPL-etching) and anodizing with sulfuric acid demonstrated better results in terms of toughness and strain to failure, while mechanical abrasion and alkaline etching had weaker interfacial bonding strength. Zheng et al. [37] in their turn reported that anodizing enhanced the shear strength by 61% when compared to mechanical treatment with sandpaper.

The influence of the surface treatment as well as the nanoparticle reinforcement can be studied with the analysis of the failure modes of the specimens after the mechanical testing. The reason is that failure type is highly important when dealing with the delamination of fiber metal laminates and primarily there are three of them:

adhesive, cohesive and mixed failure mechanisms. Adhesive failure is the failure between the adhesive and the metal, when the adhesive is stuck only on one side. Cohesive failure appears as a layer of adhesive remains on both surfaces. In a mixed failure both previous failures occur at the same time [38]. The failure mechanisms are visualized in Figure 2.3.

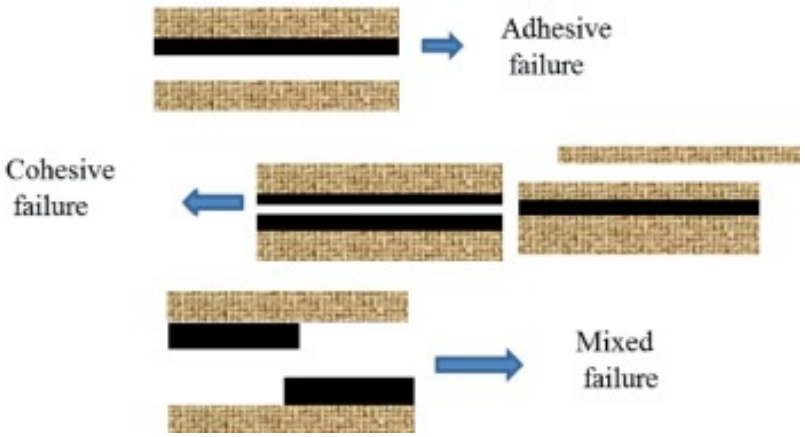

Figure 2.3. Failure mechanisms

Cohesive failure is preferred as it indicates the excellent adhesion and it is observed mainly in samples after electrochemical and chemical treatment, while mechanical abrasion specimens had adhesive failures [32, 35-37] .

The reviewed literature is directly related to our research in terms of the chosen procedure and the conducted tests. Similarly, the single-lap shear strength test and tensile strength test for pure polymer were conducted to evaluate the strength, Young's Modulus, etc. of our own samples to expand the subject.

2.2 Numerical modeling

The application of adhesives in bonded joints has increased significantly in recent years, due to its advantages over traditional joining methods, such as more efficient load transfer, the ability to conform to lightweight structures, enhanced fatigue properties, improved corrosion resistance, and smoother surfaces. There are many analytical methods for calculating stress distributions in adhesively bonded joints [39]. According to them, the maximum stress should be concentrated, where the edges of the adhesive layer are in contact with lap joints. This can be seen in Figure 2.4.

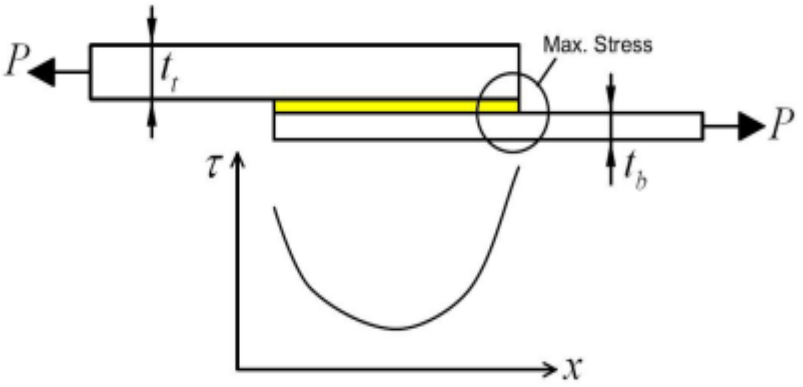

Figure 2.4. Stress distribution on the adhesive layer [39]

Besides that, it was highlighted that the plastic zone increases from the edges to the center of the adhesive layer, which is also linked with the fact that maximum stress is expected to be on the edges. In other words, failure must start at the edges (Figure 2.5) .

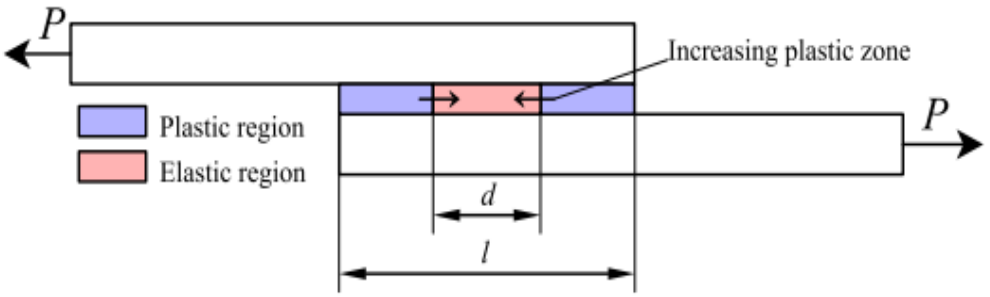

Figure 2.5. Failure in adhesive layer [39]

The single-lap joint test is usually used in research as the main one to study the displacement and failure load capacity of adhesive. So, analyzing adhesively bonded joints through both experimental and numerical methods and comparison of the results have significant importance for general understanding of their mechanical behavior [40]. A literature review reveals that finite element (FE) analyses give similar results as experimental ones in damage load, but usually, uncertainty can be observed in displacement. These differences are caused by factors such as friction between the adherend and the grips of the tensile testing device, as well as gaps between the fasteners of the devices [40]. For the numerical part, 2 models were used: the Cohesive Zone Model (CZM) and the Multilinear Isotropic Hardening model. Results showed that using cohesive zone models improves accuracy for the adhesive section, showing a

7% difference in load and a 32% difference in displacement compared to other models [40]. Due to the better accuracy of the CZM, a traction system was used for this project for the numerical part. The tensile (E) and shear (G) moduli of the adhesive, as well as, their respective strength values were known. However, researchers were unable to obtain to parameters, such as the critical strain energy release rate for mode I (G_{IC}) and mode II (G_{IIC}), which made it impossible to predict the behavior of the material under the load by using advanced modeling techniques like cohesive zone modeling (CZM) [41].

The reviewed literature is directly related to our research because the polyurethane tested in the paper had similar Young's Modulus and density properties to the ones used in this paper. Usage of the properties of SikaForceTM 7752-L60 for mode I and mode II found in one of the papers was significant since these values were not obtained experimentally.

Chapter 3

Research Methodology

3.1 Materials

Polyurethane resin

The commercial molding polyurethane PU-A80 (component A) is used for the formation of the resin. It is a white viscous liquid which immediately thickens upon contact with water. The component was sourced from the local supplier.

Hardener

The commercial molding polyurethane PU-A80 (component B) plays a role of the hardener for the polymer. It is a yellow viscous liquid. In the cured state and after mixing the components, the density of the resulting transparent yellow polyurethane is 1.18 kg/l with the shore hardness of 80 units. Similarly, the component was acquired from the local industrial market.

α - Zirconium phosphate (α-ZrP)

The α-ZrP is the nanoparticle used in the project in a form of the white powder for the reinforcement of the polyurethane adhesive polymer. α-ZrP nanoparticles were synthesized by the oxalic acid method described in the Capitani et al. [30].

Sulfuric acid

Sulfuric acid, also known as hydrogen sulfate, is a mineral strong acid with the molecular formula H_2SO_4. It is clear, colorless and soluble in a water compound that was used as an electrolyte for the anodizing process. The acid is odorless and highly corrosive for metals.

Sodium hydroxide

Sodium hydroxide is a metallic base and alkali chemical compound. It has the chemical formula NaOH. The colorless solution had a concentration of 0.2 M, after being mixed with distilled water. It served as an etching reagent to remove any contaminants.

Nitric acid

Nitric acid is a highly corrosive mineral acid that has a chemical formula of HNO_3. It is a colorless and fuming compound that was used for the secondary cleaning and surface activation.

Sandpaper

Sandpaper is an abrasive material used for roughening surfaces. In the experimental work, sandpapers with three different grit sizes (#80, #100, and #120), purchased from a local supplier, were used to treat aluminum sheets.

3.2 Experimental

3.2.1 Design of experiment

The diagram below (Figure 3.1) provides detailed information on the methods, procedures, and tests used to determine an adhesive with improved characteristics. All steps were conducted in experimental laboratories, involving different types of equipment and materials. So, the description includes information about the adhesive preparation, as well as details about the tests and testing machines.

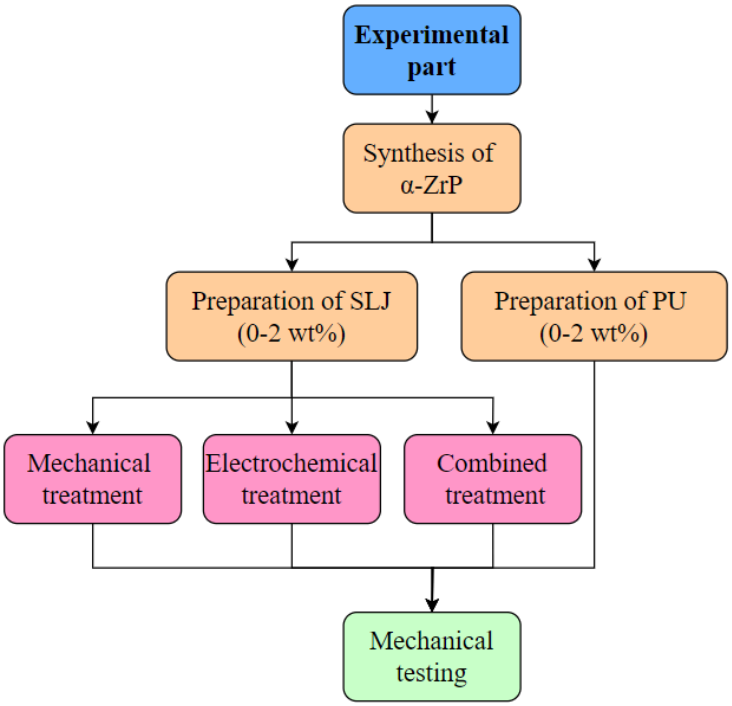

Figure 3.1. Structure of experimental design

The project primarily aims to gather data demonstrating that α-ZrP nanoparticles, along with various surface treatment methods, significantly enhance the interlayer shear strength of single lap joint specimens. The first step involves identifying the optimal nanoparticle content through mechanical testing. Next, it is important to determine the most effective treatment method among mechanical, electrochemical, or combined treatments. Lastly, to determine whether the combination

produces greater strength than individual interface enhancement procedures, the study evaluates the synergistic effect of applying surface treatment and incorporating nanomaterials with other approaches. From these data and results analysis, conclusions for the experimental part will be drawn.

The overall timeline of the experimental work and numerical modeling, with detailed periodic tasks, is illustrated in the Gantt chart below (Figure 3.2). All tasks were structured with a specific amount of time allocation in accordance with methodology of the research project.

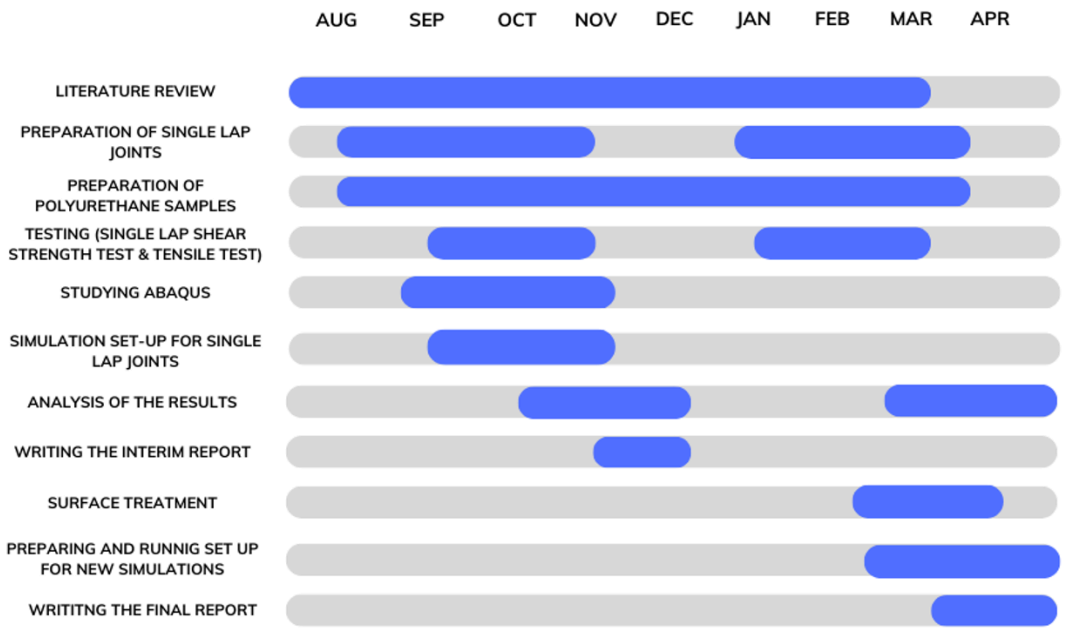

Figure 3.2. Gantt chart

3.2.2 Synthesis of α-ZrP

At room temperature zirconium oxide chloride ($ZrClO_2$) was solubilized under stirring in 35 mL of an aqueous solution of oxalic acid so that the Zr (IV) concentration was 0.1 M and the $H_2C_2O_4$/Zr molar ratio was in the range 4 to 10 (Figure 3.3). Then a 14.8 M of H_3PO_4 was added so that the H_3PO_4/Zr molar ratio was in the range 2 to 6. The resulting solution was heated for 24 h at 80°C. Then the obtained precipitate was separated from the solution by centrifugation at 3000 rpm and washed three times with 10^{-3} M of HCl. Everything was left to dry overnight at 80°C in vacuum oven and then grinded to have a powder of α-ZrP [30].

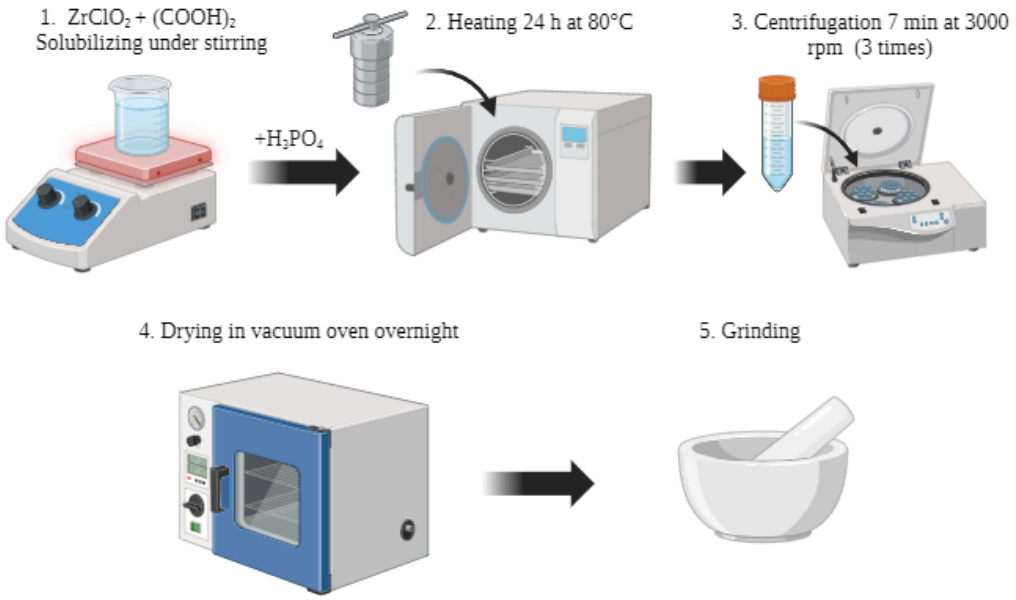

Figure 3.3. Synthesis of α-ZrP

3.2.3 Specimen fabrication procedure

The component A (8.5 g) of PU-A80 is mixed with a calculated amount of nanomaterials using magnetic stirring with speed of 300 rpm for 20 minutes at room temperature. Then, the component B (8.5 g) of PU-A80 is added to the mixture and everything is stirred for 3 minutes. After that, the adhesive is applied to aluminum sheets with the brush and the samples are pressed on both sides with paper clips to maintain consistency in adhesive thickness and restrict the motion of sheets until the adhesive is fully cured. Then single lap joint specimens are cured under a fume to avoid occurrence of bubbles in the samples. The remaining polyurethane is poured into steel mold for the preparation of pure polymer samples (Figure 3.4). In the end four SLJ and four pure polyurethane samples were made for the further mechanical testing.

If surface treatment is required, it is applied to the aluminum sheets before the adhesive application step.

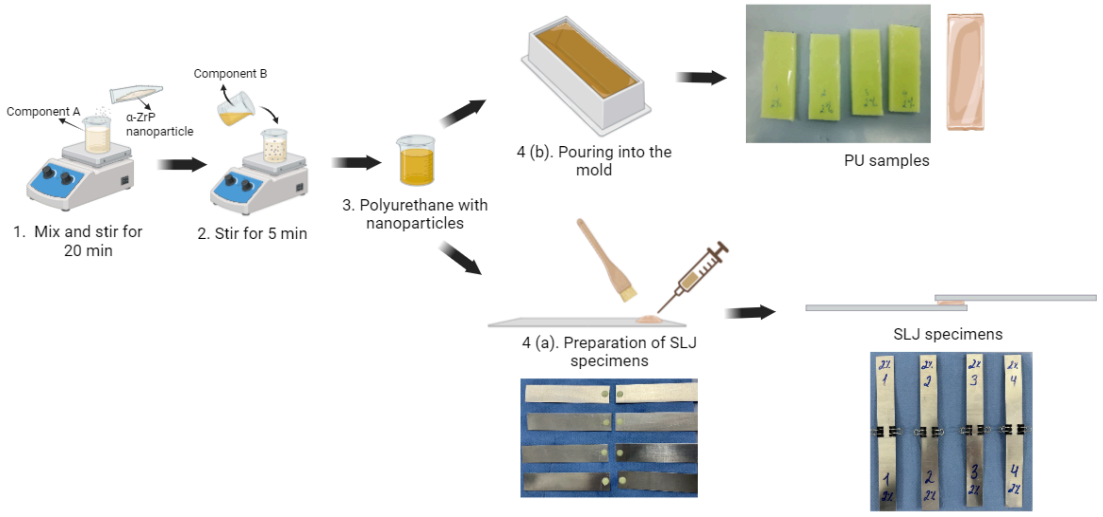

Figure 3.4. The preparation of SLJ and polyurethane samples

3.2.4 Calculations

The calculations for the mass of the nanomaterial corresponding to the certain weight percentage and the overall mass of components A and B are determined by the following formulas.

$$m_{solution} = m_A + m_B + m_{ZrP} \quad (1)$$

$$\text{Mass \% of α-ZrP in this solution} = \frac{M_{ZrP}}{m_{solution}} \times 100\% \quad (2)$$

To built stress-strain graph for tensile test the following formulas were used:

$$\varepsilon = \frac{\Delta d}{D_0} \quad (3)$$

Where, Δd stands for displacement [mm], D_0 is initial length of sample [mm] and ε is a strain.

$$\sigma = \frac{F}{A_0} \quad (4)$$

Where, F stands for Load [N], A_0 is initial cross sectional area of sample [mm^2] and σ is stress [MPa].

In order to identify Young's Modulus, it is significant to determine the linear part of the stress-strain curve, plotted by using formulas 3 and 4. By choosing two points on the linear region on the curve, the Young's Modulus (E) can be calculated by using the following equation:

$$E = \frac{\Delta \sigma}{\Delta \varepsilon} \quad (5)$$

Where, Δσ stands for difference in stress between chosen points [MPa], Δε difference in strain between chosen points and *E* is Young's Modulus [MPa].

3.2.5 Surface treatment

Mechanical treatment

One of the surface treatment methods used in this research is mechanical surface treatment. The step-by-step procedure and initial setup, along with all necessary dimensions, are shown in the diagram below (Figure 3.5). Initially, the aluminum sample is placed on the designated spot on the wall, as indicated in the diagram. Then, using a screwdriver with sandpaper connected to it, pressure is applied at full power for 10 seconds to roughen the surface of the sheet. For the roughening process, sandpaper with three different grit sizes was used: 80, 100, and 120. These processes were repeated for every sheet that was used for testing the effect of mechanical treatment on interface strength.

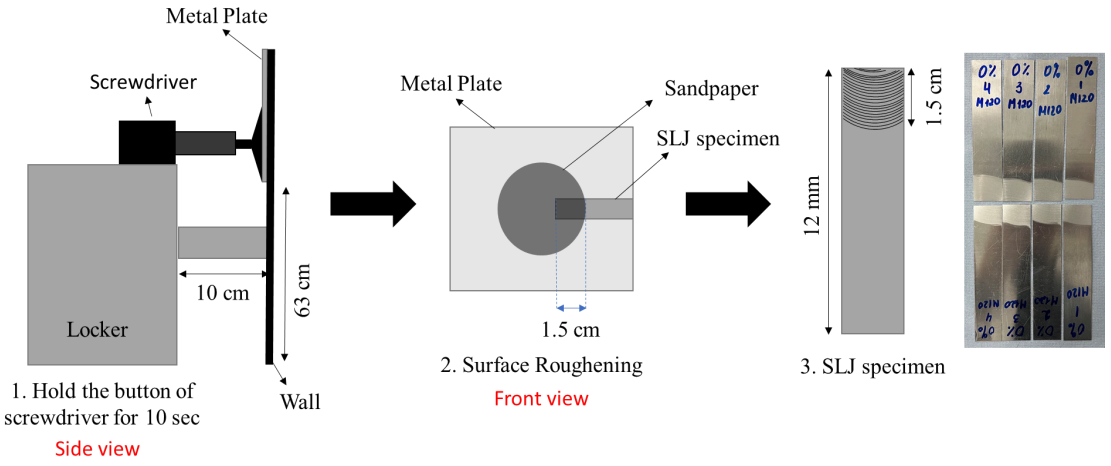

Figure 3.5. Mechanical surface treatment setup

Electrochemical treatment

For the electrochemical treatment anodizing process was performed. As it is shown in Figure 3.6, the aluminum sample was degreased in 20 ml of ethanol such that about 15 mm of the metal was immersed in the solution. Then the etching is performed with 20 ml of NaOH (0.2 M) for 2 minutes and after that the sample is subjected into 20 ml of HNO_3 (1 M) for 1 minute. The anodizing is performed in 100 ml of H_2SO_4 (0.5 M) solution using the DC Power supply GW Instek GPS-18500. The red wire (anode) was connected to the platinum electrode, while the black one (cathode) was connected to the aluminum sample. After 45 min the sample is subjected into ethanol for a few

minutes and then dried in a vacuum oven for 15-20 min. The solutions were replaced after 5 samples each time.

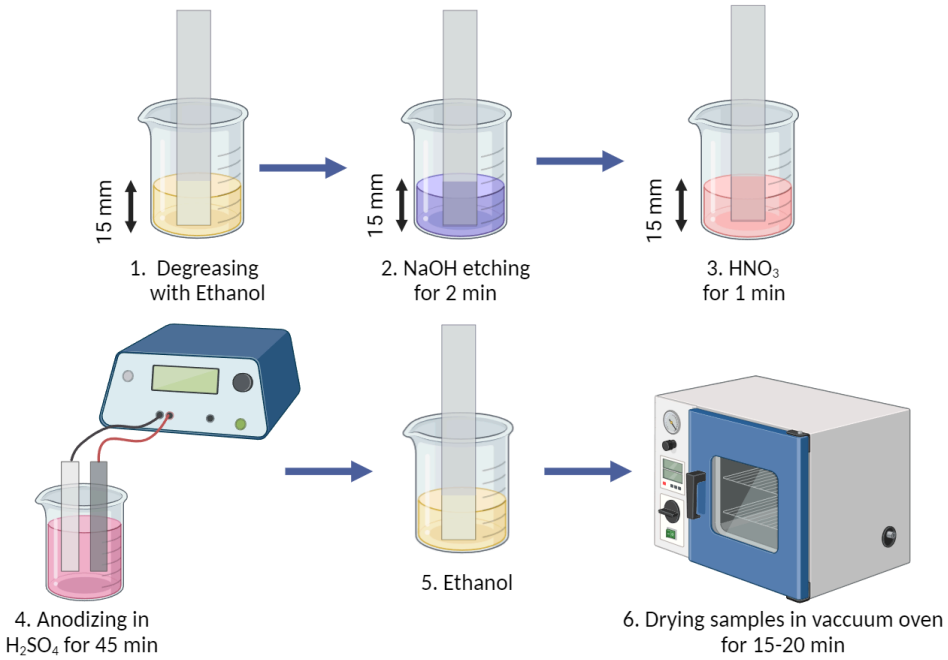

Figure 3.6. Anodizing procedure

Table 3.1. Specimen's code

Specimen	**Code**
No treatment and no reinforcement (0 wt% of α-ZrP)	REF
Mechanical treatment (grit size M#)	M80, M100, M120
Electrochemical treatment	EC

3.2.6 Testing procedure

Single-lap shear strength test

The Single-lap shear strength test measures an adhesive's shear strength on a single-lap joint specimen in order to determine its suitability for bonding metals. In the study, the test was applied for assessment of single lap joint samples prepared with both pure polymer and polymer containing nanoparticles. The experimental measurements were conducted using a Universal Testing Machine, as illustrated in Figure 3.7 (a)**.** Lap shear strength test setup and the testing conditions were setted in accordance with ASTM D-1002 standard of Lap Shear Strength of Adhesively Bonded Metal

Specimens. Figure 3.7 (c) show the dimensions of the single-lap shear strength test specimens.

Tensile strength test for polymer:

In tensile strength testing, a sample is pulled apart until it breaks, and the tensile strength is determined by measuring the required force. To ensure the integrity of the material and understand the mechanical characteristics of pure polyurethane, tension tests are conducted to identify the point of failure across the testing sample. The machine used for tensile strength testing is Tensile Tester and is illustrated in Figure 3.7 (b). The tests were conducted in accordance with ASTM 412 Standard, which is the Tensile Test on Rubber and Elastomer (tensile (tension) properties of vulcanized thermoset rubber and thermoplastic elastomers). Figure 3.7 (d) show the dimensions of the tensile test sample.

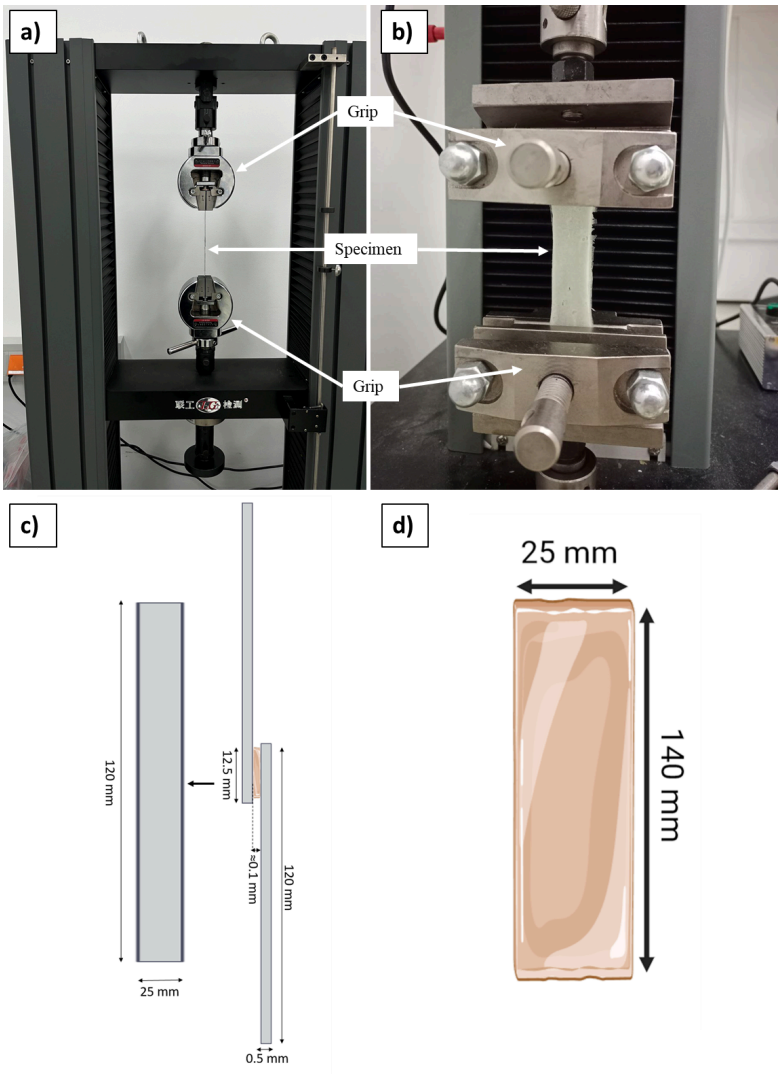

Figure 3.7. Testing equipment: a) Lap shear strength test setup, b) Tensile Tester; and Dimensions of specimen: c) SLJ, d) PU

3.3 Numerical

3.3.1 Design of numerical simulation

The project includes a numerical simulation component, the results of which support the experimental data. Moreover, it provides detailed insight into load transfer mechanisms within the material, highlighting stress concentration regions and demonstrating how materials deform under specific stress levels. Based on the obtained data, it is possible to predict potential failure modes and analyze material properties. Abaqus software is employed for the numerical simulation model. The numerical simulation plan is summarized in the chart below (Figure 3.8).

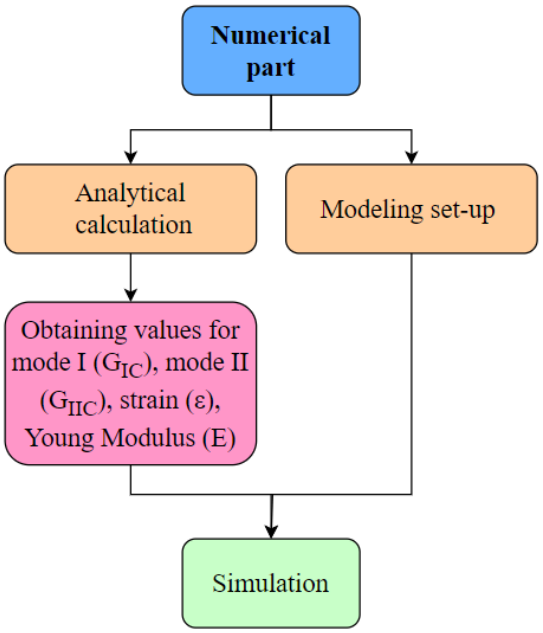

Figure 3.8. Numerical modeling stages

The first step involves identifying values and properties of the materials engaged in the simulation. To do that, it is necessary to analyze the data, obtained by experimental parts. By doing so, Young's modulus was identified by using calculation from the experimental part. Besides, it was significant to search for data, which could not be found experimentally, such as energy release rate for different modes (I and II). After that, these values can be used to calculate the parameters used in simulation. Moreover, there is a need to set-up the model properly to get required results. Modeling set-up consists of choosing proper meshing, boundary conditions, geometry of all parts and time increments' size. Finally, the simulation can be tested and results can be compared with the experimental one.

3.3.2 Simulation setup for SLJ

2D parts were decided to be used for simulation due to the simplicity of the single lap joint test. In other words, 2D elements require less computational resources compared to 3D ones, while presenting data with necessary accuracy for this research. The model consists of one 2D "Shell planar" part, but divided into sections: "cohesive" and "Solid, Homogeneous". It is divided into these sections to test the elongation properties of an adhesive material which is a "cohesive" section. By using dimensions from the experimental part, the parts' sketch was drawn. The thickness of the metal plates were taken as 0.51 mm and length as 100 mm, which is the size of the ones used in experiments (Figure 3.9).

Reference point was used to define the Load parameters: the right one was defined for elongation with 60 mm/s speed uniformly distributed over right edge length (Figure 3.9), which is equal to the one used for experiment works. Boundary conditions were set as follows: we had zero degrees of freedom at the left side of the upper lap (Figure 3.9).

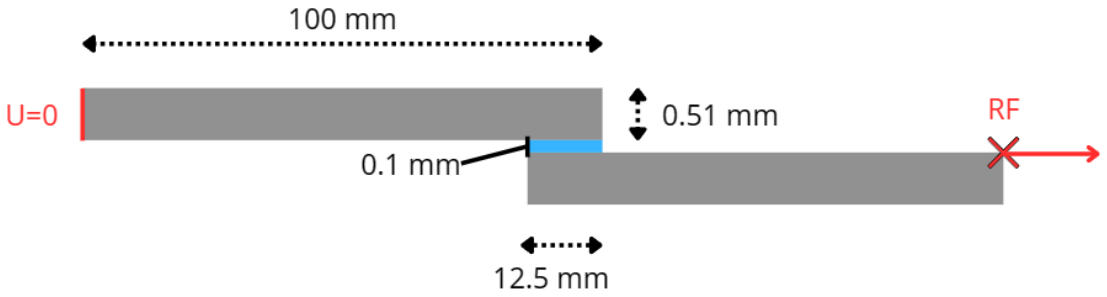

Figure 3.9. Setup for SLJ

3.3.3 Simulation parameters

The following mechanical properties were set for a specimen for conducting simulations:

- Elastic properties of solid sections: Young's modulus & Poisson's ratio
- Elastic properties of cohesive sections: Traction values
- Quad damage properties: Nominal stress at first and second directions and normal-only mode one
- Damage evolution: Linear displacement at failure

Due to experimental issues, values for G_{IC},$G_{IIC}$and σ_{IC},σ_{IIC} were taken from the source described in the literature review. σ_{IC} and σ_{IIC} are values of strength in mode I

and mode II. G_{IC},G_{IIC} are values of critical strain energy release rates for mode I and mode II.

Table 3.2. Values needed to find coefficients for simulation

E	G_{IC}	G_{IIC}	h
288.9 MPa [our work]	23.13 MPa[41]	54.8 MPa [41]	0.1 mm [our work]

Values for simulation elastic traction parameters were calculated by dividing critical strain energy release rates by the thickness of the cohesive layer in a single lap joint test:

$$G_1 = \frac{G_{IC}}{h} \quad (5)$$

$$G_2 = \frac{G_{IIC}}{h} \quad (6)$$

$$E_n = \frac{E}{h} \quad (7)$$

Where, h is the thickness of the cohesive layer in a single lap joint test.

Quads' damage properties were taken as strength values from a single lap joint test. Finally, the coefficient for damage evolution was calculated by multiplying displacement at failure to the strength of the adhesive.

$$D_n = \tau * \delta_n^{fail} \quad (8)$$

Since, mode II and mode III, properties are usually have very close values, it was decided to use σ_{IIC} value also as a strength in mode III.

Table 3.3. Values for Simulation for lap joint test of polyethylene with 0 wt% α-ZrP

E_n	G_1	G_2	D_n	σ_{IC}	σ_{IIC}, σ_{IIIC}
2889	23.13	54.8 [41]	0.388	5.79 MPa [41]	1.48 MPa [41]

3.3.4 Meshing

The constant mesh size was used for the whole part. In order to minimize the time spent on each simulation, while getting accurate results, 0.1 was chosen as a global size for mesh. Different meshes in the vertical direction for the adhesive layer zone

were tested for this model. The number of elements in the vertical direction varied from 1 to 3 for different models.

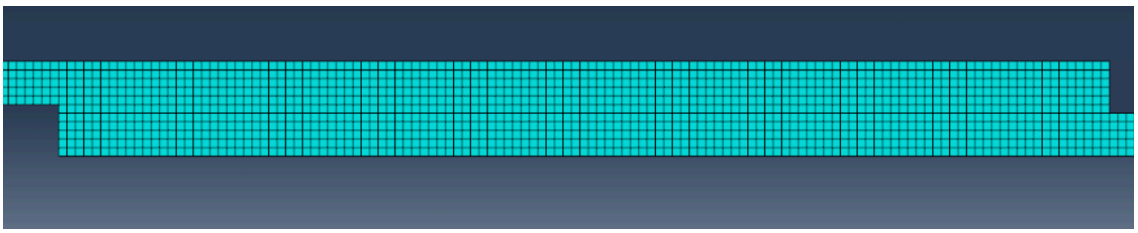

Figure 3.10. Meshing of Part with 1 element in vertical direction

Table 3.4. Different meshings for simulation

Elements number in vertical direction	Minimum size of the element	Number of elements in cohesive region
1	0.1	250
2	0.05	500
3	0.03	750

After running a few simulations, it was noticed that meshing with 1 element in vertical direction gives much more stable results, while it also allowed to build load-displacement graphs till failure of lap joint, while simulation with smaller vertical meshing size result shows deformation process only till elongation reaches 0.1 mm. The instability and inability to show the total deformation process of simulation with smaller vertical mesh size, is linked with requirement for much smaller time step and increments in comparison to the one we used. Due to that, it was decided to use meshing with 1 element in vertical direction.

Table 3.5. Different meshings for simulation

Minimum size of the element	Number of elements in the whole model
0.1	10125
0.05	11500
0.03	13337

Different meshes in the horizontal direction for the central zone were tested for this model. The number of elements in the vertical direction varied from 1 to 3 for different models. After running a few simulations, it was noticed that results of the

simulation are independent of element size in horizontal direction. The only difference is the fact that simulation took much longer time for running with the smaller meshing. Based on this, it was decided to use meshing with 0.1, which was chosen as a global size.

Chapter 4

Results and discussion

4.1 Characteristics of α-ZrP

For the purpose of the experimental work, α-ZrP was synthesized according to the methods described in the methodology. In order to obtain material characteristics results the Fourier Transform Infrared Spectroscopy (FTIR) technique was utilized as identification methods, demonstrating the compatibility of the synthesized ZrP nanoparticle with data from the material database (Figure 4.1). Also, Scanning Electron Microscopy (SEM) was done to provide a detailed view of the nanoparticles, revealing their microstructure and visual characteristics (Figure 4.2).

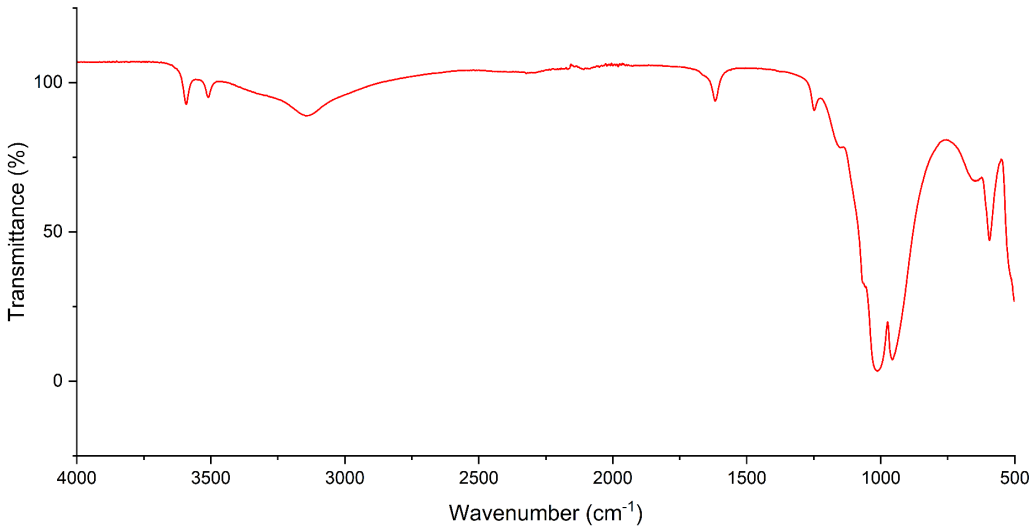

Figure 4.1. FTIR spectra of α-ZrP

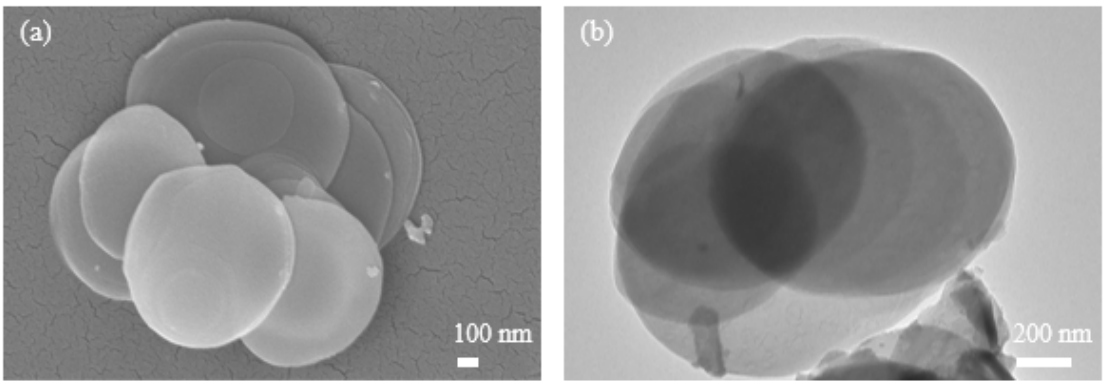

Figure 4.2. SEM images of α-ZrP a) 100 nm b) 200 nm

4.2 Tensile properties

The tensile strength testing was performed in order to obtain necessary information about the produced adhesive material. According to gathered data (Figure 4.3 (a) and Table 4.1) tensile strength and modulus of the commercial polyurethane shows significant increase after incorporation of the 0.5 wt% of nanomaterial, reaching the peak value with 1.0 wt%. In particular, the polymers containing 1.0 wt% α-ZrP showed an average tensile strength and modulus of 28.2 MPa and 519.15 MPa, respectively, representing approximately 3.5 and 0.8 times improvements compared to pure polyurethane (0.0 wt%) without any reinforcing agent. Addition of nanomaterials with their even dispersion in the polymer matrix, enables effective stress distribution within material [3, 42]. Improved stress transfer is achieved through the properties of α-ZrP nanoparticles, which have a high surface area relative to their volume, enabling a larger area for interaction and providing a more even stress distribution from the polymer to the stiffer nanoparticles [43, 44]. Since the nanoparticles operate as an obstacle, the α-ZrP was the main factor of the polymer's high tensile performance and increased deformation resistance. However, with the addition of more α-ZrP into the polymer, exceeding a certain threshold, a gradual decrease in strength and tensile modulus can be observed for polymers containing 1.5-2 wt% α-ZrP. Although experimental results indicate a declining trend for these parameters, with decreases of approximately 11.5% and 35.5% respectively compared to those with 1 wt%, they still provide higher values than the control sample. Possibly, it is due to the agglomeration process, when attractive forces, such as van der Waals forces, start clustering nanoparticles together, creating a number of higher localized stress points. As a result, it weakens the material [42].

Correspondingly, Figure 4.3 b illustrates that with the rise in the concentration of nanomaterial, the maximum stress also appears to increase, signifying that nanoparticles enhance the overall material strength, enabling it to withstand higher forces. Moreover, the smoothness and similarity of the curves suggest consistent experimental results and effective dispersion of the nanomaterial. The increased strain not only indicates higher ductility and toughness but is also reflected in the larger area under the curve, implying that the material can attain greater elongation at break and absorb more energy. Furthermore, the graph shows that the curves get steeper as the

weight percentage (wt%) increases. This steepness means that the material has become more resistant to deformation, demonstrating an increase in the elastic modulus.

Since the purpose of the tests is to find the most efficient concentration of α-ZrP, which provides the highest tensile properties of the material, it is evident that introduction of 1 wt% of nanoparticles produces the stiffest and strongest material. Kale et al. [45] also reported such concentration (1 wt%) to have the highest tensile strength in their study, where they reinforced the waterborne polyurethane with the amine intercalated α-zirconium phosphate. In their work tensile strength value was about 25 MPa, while in our case it was 28.2 MP, meaning results reveal similar tendency in findings.

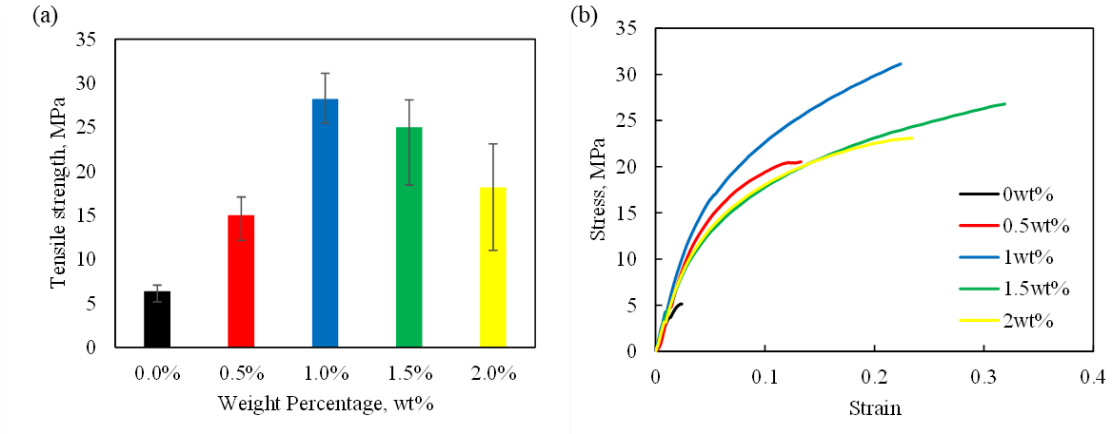

Figure 4.3. a) Tensile strength and b) Stress-strain graphs for commercial pure polymer samples

Table 4.1. Young's Modulus (E) values in MPa

n	E(0 wt%)	E(0.5 wt%)	E(1 wt%)	E(1.5 wt%)	E(2 wt%)
Sample 1	289.37	521.42	435.20	350.87	411.69
Sample 2	298.30	385.60	611.24	500.50	280.73
Sample 3	279.81	334.43	540.76	396.13	478.72
Sample 4	288.11	350.78	489.40	344.79	426.80
Average	288.90	398.06	519.15	398.07	399.48

4.3 Single lap joints

Figure 4.6 (a) depicts the average results of the calculated interlaminar shear strength (ILSS) values of the single lap joints with varying concentrations of

nanoparticles. The bar chart clearly indicates a substantial enhancement in shear strength upon the addition of α-ZrP. Specifically, specimens incorporating 0.5 wt% of the nanomaterial demonstrate the highest strength, while those with 1 wt% and 1.5 wt% show comparable improvements, with approximately 91.8%, 74.1%, and 78.4% enhancements in strength, respectively, compared to the reference sample. The use of nanomaterials allows for the development of robust interfaces, leading to improved interfacial bonding between materials. Interestingly, the sample with 2 wt% exhibits a strength value almost identical to that of the reference sample. Therefore, it is suggested that adding more nanoparticles resulted in a decrease in shear strength of the samples, due to the clusters formation among α-ZrP particles. Khurram et al. [22] had the similar behavior in their results and reported that this could be due to the increase of the viscosity of the epoxy resin at higher concentrations. Similarly this could be our case too such that increase in the concentration of the nanoparticles significantly impacts the bonding ability of the polyurethane to the aluminum sheets, hindering the penetration of the polyurethane on the pores of the metal.

Overall the tests yielded even better results compared to the data presented by Askin and Touren [27], who observed only a 24% maximum increase. This variance could be attributed to their use of different nanoparticles, such as graphene platelets (GnPs). Nevertheless, the overall trend of the results remains consistent, supporting the fact that nanoparticles can effectively reinforce material properties and their concentration play a critical role in determining the shear strength.

Using this testing method, the bonding strength between an adherend (aluminum sheet) and an adhesive (polymer) can be assessed. Interlaminar cracking, a common sign of a strong bonding mechanism in these shear studies, indicates successful adhesive properties. However, achieving pure shear failure, particularly in the adhesive's central plane, remains challenging as shear failure doesn't always occur there [46]. This difficulty in achieving predictable failure patterns underscores the significance of the experimental results, which revealed that despite an overall increase in mechanical properties, adhesive failure was still prevalent in most samples. It's interesting to note that cohesive failure, indicating superior interlocking, was mostly seen when the adhesive was strengthened with 2 wt% of α-ZrP nanoparticles, underscoring their impact on changing failure modes. The comparison of the failure mechanisms between 0.5 wt% and 2 wt% is illustrated in the Figure 4.4 below. As can

be seen, specimen a) experienced adhesive failure, while specimen b) exhibited a small cohesive region.

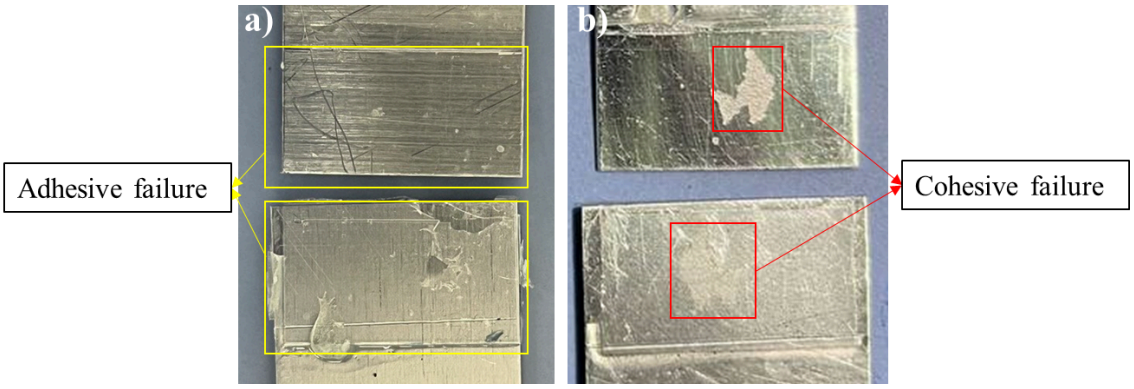

Figure 4.4. Failure mechanisms of a) 0.5 wt%, b) 2 wt%

SEM images focusing on the damaged area after the shear test are shown in Figure 4.5. These images showcase the failed response of the material after testing. Although the 0.5 wt% specimen exhibited adhesive failure, the images reveal slight indications of an adhesive pull-out mechanism. This mechanism is a condition where the adhesive layer deforms or detaches from the substrate, which might leave adhesive residue on aluminum surfaces after failure. Such pull-out is a sign that the polymer and metal had strong adhesion, possibly stronger than the cohesive forces inside the adhesive material itself. At the failure point, the adhesive pulls out of the substrate rather than simply detaching (adhesive failure).

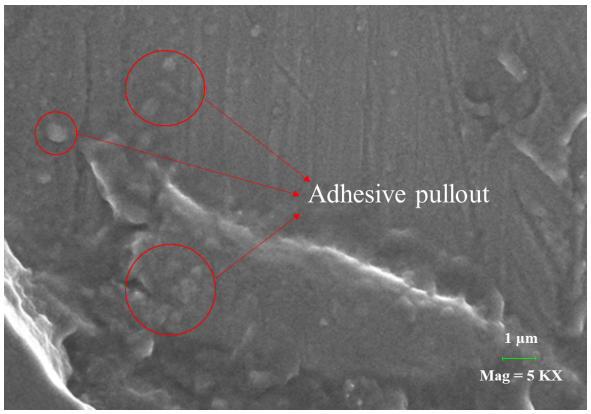

Figure 4.5. SEM images of surfaces of 0.5wt% sample after testing

Analyzing Figure 4.6 (b), it can be noted that the polymer containing 0.5 wt% of α-ZrP also exhibits the best elongation results and greater area under the curve indicating more energy absorbed. Overall, the graph demonstrates similar trends, showing that the addition of nanoparticles enhances the samples' ability to withstand

forces. As the nanoparticle content approaches 1.5 wt%, the gradient angle increases, indicating poorer elongation characteristics. However, even with the addition of 2.0 wt% of α-ZrP, which exhibits higher results compared to the reference sample, the elongation characteristics still decline. Similar findings were obtained by Khurram et al. [22] with MWCNTs nanomaterial, which show that the strength of FMLs are better when they added 2.0 wt% of MWCNTs and further implementation of the nanoparticles resulted in a decrease of the strength.

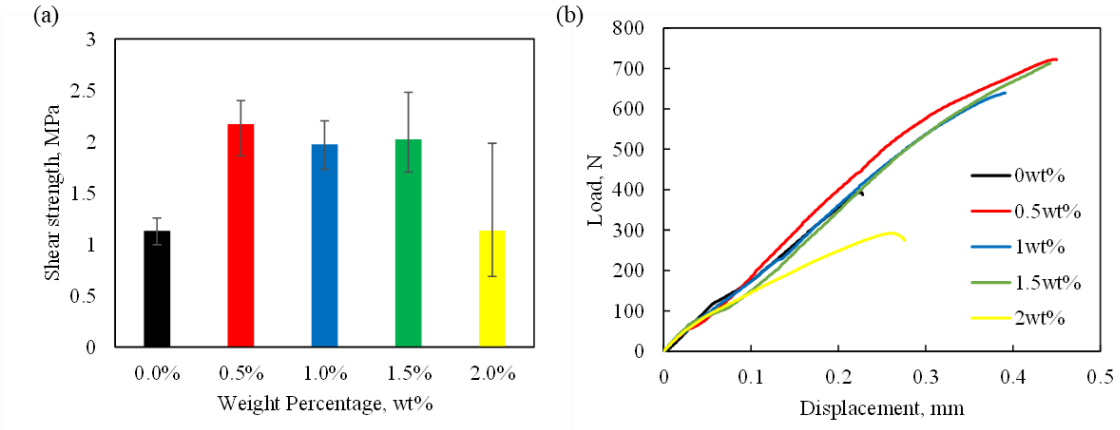

Figure 4.6. a) Strength vs percentage graph for SLJ, b) Load vs displacement curve for SLJ

4.4 Effect of surface treatment

Mechanical treatment

In Figure 4.7 (a) the surface roughness of the untreated reference sample is shown. The heights of the peaks are relatively similar and the frequency is high, which shows that the surface of the aluminum is relatively smooth. Treating the samples with sandpapers created a new surface which has higher peaks and lower frequency of their placement. Even though M100 had the highest peak in Figure 4.7, the surface structure is not symmetrical and uniform from both sides which could create some difficulties and non-uniformity of the bonding layer. Compared to it, M80 and M120 showed better results with more or less symmetrical roughness structure along the sample surface.

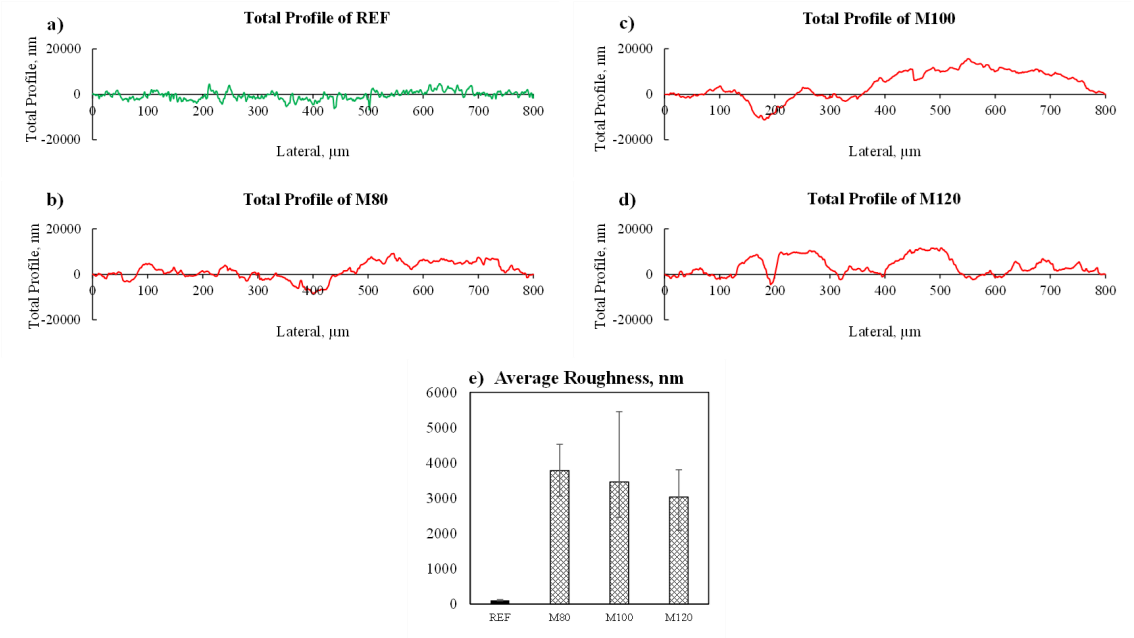

Figure 4.7. Total roughness profile for: a) Untreated aluminum surface, b) M80, c) M100, d) M120; e) Average roughness of all samples

Electrochemical treatment

The total roughness profiles are given in Figure 4.8, where Figure 4.8 (a) is the roughness of the reference sample that experienced no surface treatment at all and Figure 4.8 (b) corresponds to the sample that underwent electrochemical treatment. On average the peaks of EC samples are greater and there is more roughness in Figure 4.8 (b), which results in more space where the adhesive can interlock. This shows that the anodizing process created the roughness on a microscopic level, improving the bonding between the metal and the adhesive layer.

In Figure 4.8 (c) it is clear that the surface has been roughened and the average roughness of the treatment is 167.2 nm which is 60 nm more than that of the reference sample.

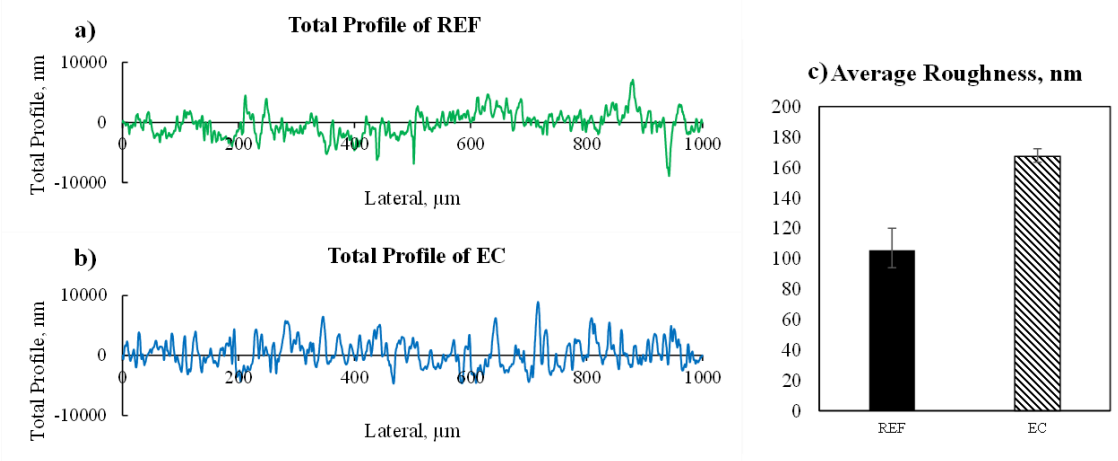

Figure 4.8. Total profile for a) Reference sample, b) EC sample

Comparison of mechanical and electrochemical treatments

In general, the introduction the surface treatment had a positive effect on both the strength and elongation properties of the adhesive polymer in the single lap joints (Figure 4.9). This improvement resulted due to enhanced interlocking mechanisms providing the adhesive with greater bonding area. The mechanical treatment enhanced the shear strength of the specimens by about 35%. The electrochemical treatment showed the best results, even greater than for mechanical abrasion. This could be due to the fact that the anodizing process provides less microroughness than for sandpaper treatment which is more preferable for better bonding of the adhesive layer to the metal. Indeed, comparing Figure 4.7 and Figure 4.8 the average roughness of the electrochemical treatment is much less than that of mechanical one, 167.2 nm and 3037.34 nm respectively. The results also correspond with the findings of Aghamohammadi et al. [32] and Zheng et al. [37], who found that samples that underwent anodizing process had better strength results than those after mechanical treatment. Electrochemical process improved the shear strength by 174% when compared to another treatment, which is much higher than Zheng et al. 's [37] results, who had only a 61% increase. The difference could result due to the fact that researchers used magnesium alloy, not aluminum as in our case and they had another grit size of the sandpaper. However, the overall tendency of the results is similar.

According to Figure 4.9 (b), EC and M120 samples stand out from the other results. Interestingly, EC samples can withstand greater loads, while M120 has better elongation. However, the areas under these two curves are approximately the same

meaning that they absorb a similar amount of energy. This drives us to the conclusion that anodizing process can enhance load-bearing capabilities, but it could not significantly improve elongation characteristics of the material. Similarly, mechanically treated samples may not withstand greater loads as electrochemically treated ones, but certainly their ability to elongate could be efficient for some applications, where it plays a crucial role.

For mechanical treatment the best grit size was identified to be #120 (Figure 4.9). However, in Figure 4.7 (e) M120 has the lowest average roughness value and this contradicts with the findings of Mohammad et al [33], who reported that sanpapers with higher roughness had better enhancement of the strength of the composite material. It is worth noting that in this work, the difference between the grit sizes of the sandpaper is greater than in our project, and the method of using sandpaper as well as the material was different. This could give such different results. Moreover, according to the Pan et al. [47] the shear strength of the specimens vary only slightly when different grit sizes are applied. Similarly, our sandpapers' grit sizes differed only by 20 and expectedly the results of the average roughness along with the values of shear strengths are pretty close. Average roughness values are all in a range of 3-3.7 μm, while the shear strengths' values are approximately the same 1.3-1.5 MPa. That is why it is better to use big intervals between the grit sizes to see more dramatic changes.

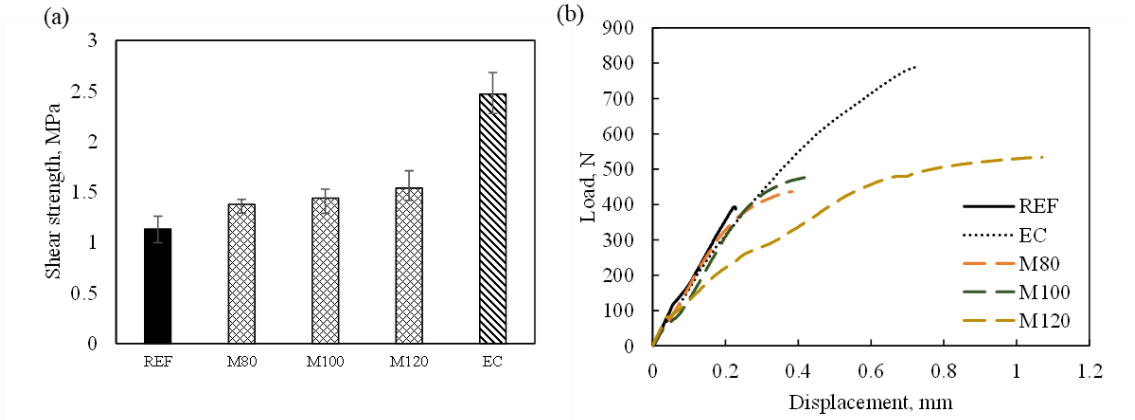

Figure 4.9. The effect of different surface treatment on the a) shear strength (0 wt%), b) displacement of 0 wt% samples

The effectiveness of the adhesive of electrochemically treated sample can also be seen from Figure 4.10 where the failure mechanism of the samples is shown. Compared with the failure fracture of the reference sample in Figure 4.10 (a), the

adhesive is present on both surfaces of the single lap joint in Figure 4.10 (b) and this gives the cohesive type of the failure. The result corresponds to the literature, where the researchers also found that electrochemical treatment can give a cohesive failure, showing greater results for interfacial bonding [32, 35-37]. The mechanical treatment did not show any improvements in the failure mechanism compared to the reference sample, also having an adhesive type of the failure (Figure 4.10 (c)).

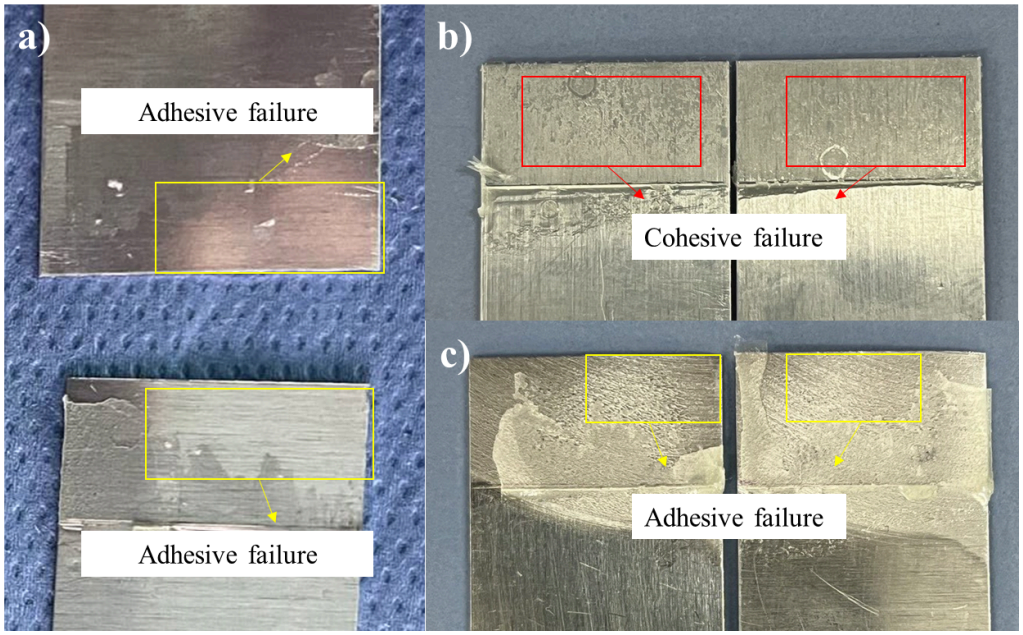

Figure 4.10. Failure mechanisms of a) REF, b) EC, c) M120

4.5 Synergetic effect of surface treatment and α-ZrP

Mechanical treatment with α-ZrP

Mechanical treatment combined with α-ZrP showed higher results for the shear strength of the samples than for pure sandpaper abrasion. The tendency of the improvement of the strength starting from grit size #80 to #120 remained the same such that samples with lower roughness (M120) had better ability to withstand loads. Comparing with the reference sample (0 wt%) the shear strength of the M80, M100 and M120 specimens increased by 69.6%, 73.7% and 81.5% respectively.

However, all these values were lower than the shear strength of the nano-reinforced sample with 0.5 wt% of α-ZrP. As discussed earlier, mechanical treatment provides even more roughness that could be seen by the naked eye. So, the presence of nanoparticles only weakened the specimens because they agglomerated and

got stuck in wider pores not bonding efficiently with the metal surface. Moreover, all the samples had adhesive failures (Figure 4.12 (a)).

Electrochemical treatment with α-ZrP

Combining the electrochemical surface treatment with α-ZrP gave even better data, having the result of 5.6 MPa shear strength which is much higher than that of the reference samples. The strength was increased by 398.3% compared with 0 wt% and by 159.8% compared with the nano reinforced sample (0.5 wt%). Also, the ability to withstand greater loads improved significantly compared to EC specimens (0 wt%), which means that microroughness enhanced the interlocking mechanism and nanoparticles hindered the crack propagation.

According to Figure 4.11 (b), EC samples can withstand the greatest load and show the best elongation result with highest absorption of the energy. So, incorporating the α-ZrP nanoparticles not only increased the load-bearing capability but enhanced the elongation results compared to the 0 wt% treatment values (Figure 4.9 (b)). So nanoparticles effectively dispersed in polyurethane matrix, hindering the crack propagation and deformation under the load. They also affected the deformation mechanism and the material's resistance to fracture, enabling the polymer to deform even more before reaching the ultimate strength. So, the treatment and reinforcement are compatible, showing that synergistic effect positively affects the mechanical properties of the single lap shear specimens (Figure 4.11).

Moreover, studying the failure type of the single lap joints showed that electrochemical treatment with α-ZrP has a mixed failure mechanism. According to Figure 4.12(b) the adhesive and cohesive failures occurred simultaneously.

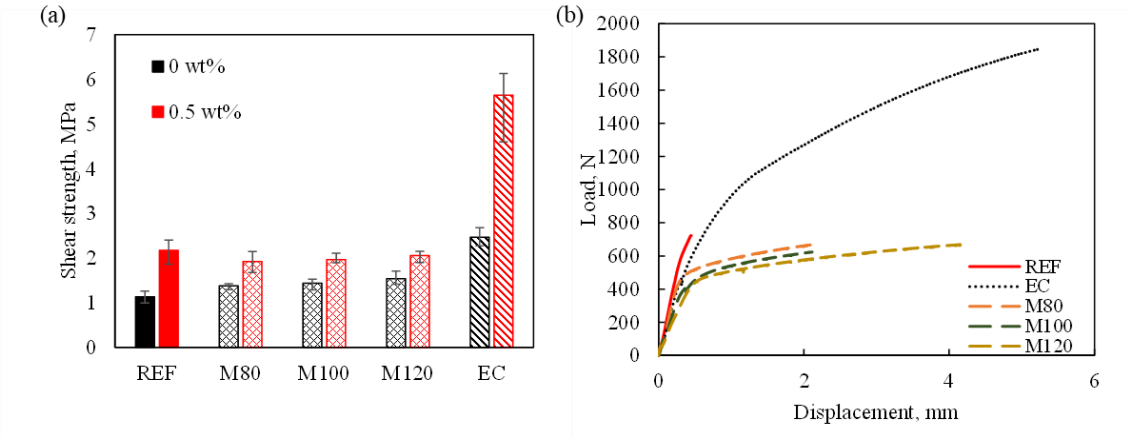

Figure 4.11. Effect of different treatment types on a) the shear strength (0 wt% and 0.5 wt%), b) displacement of the 0.5 wt% samples

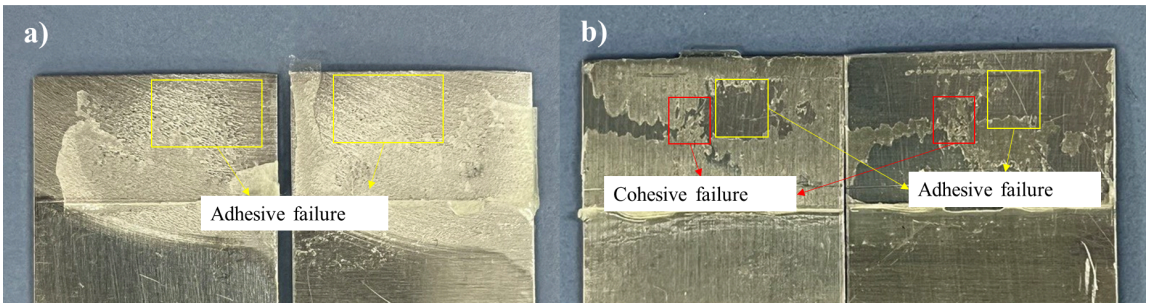

Figure 4.12. The failure mode of a) M120 (0.5 wt%), b) EC (0.5 wt%) sample

The surface morphology of the samples were obtained and Figure 4.13 (a,b) shows the surface of the untreated reference sample and Figure 4.13 (c-h) show the samples treated with different methods. Compared to the smooth surface of the aluminum, the mechanically treated (M120) and electrochemically treated (EC) samples have visible roughness.

In Figure 4.13 (e), the mechanically treated specimen has scratches going in one direction, while in Figure 4.13 (g) the surface has a porous structure of an oxide layer formed by anodizing, which also corresponds to the findings in literature [34]. It is clear that there is less adhesive on the smooth surface of the metal, while more polymer has remained on the aluminum due to scratches and pores.

Importantly, the nanoparticles gather at the surface of the metal hindering the polyurethane from penetrating to the large scratches (Figure 4.11(f)). They agglomerate and stick together creating some air gaps. Due to this the polyurethane cannot bond effectively to the metal surface and some of its torn pieces are seen in SEM image (Figure 4.11(e)). On the contrary, the cavities created by the anodizing process are too

small to allow the nanoparticles interfere with the bonding, which helps in eliminating the air gaps in the pores. They also do not agglomerate on the surface of the metal and the reinforcing agent is more uniformly dispersed in the polymer (Figure 4.11 (h)). That is why the interlocking is strong between the adhesive and the metal and the polyurethane connected to the pores undergoes more elongation (Figure 4.11(g)), so that more force was needed to pull and break the sample. Compared to it, the polymer on the mechanically treated surface is not evenly widespread, which implies less stress distributed along the adhesive compared with the electrochemically treated case. Consequently, the polymer structure is less stretched compared to the anodizing surface, so EC samples can withstand more force than M120 samples.

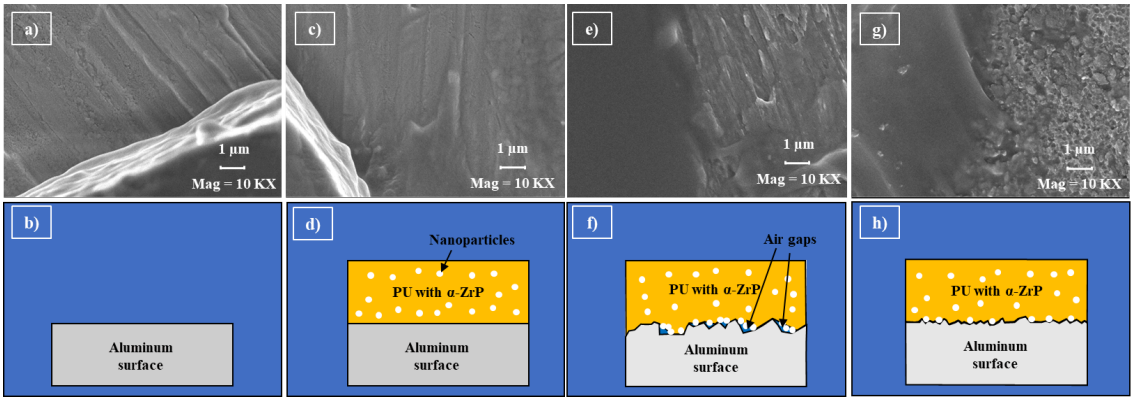

Figure 4.13 a) SEM of aluminum surface, b) Schematics of aluminum surface, c)SEM of REF (0.5wt%) sample after testing, d) Aluminum surface with applied polyurethane with nanoparticles, e) SEM of M120 (0.5 wt%) sample after testing, f) Mechanically treated aluminum surface with applied polyurethane with nanoparticles, g) SEM of EC (0.5 wt%) after testing, h) Electrochemically treated aluminum surface with applied polyurethane with nanoparticles

Mechanical and electrochemical treatment with α-ZrP

Combining electrochemical treatment, mechanical treatment and reinforcement with nanoparticles increased the shear strength by 18.9% and 25.6%, compared to the reference sample (0.5 wt%) and M120 respectively. However, combined treatment's results were weaker than data for nano reinforced anodizing process (Figure 4.14(a)). EC sample's shear strength is greater than that of the combined one by 118.6%. Even though its ability to withstand greater load was not improved, the elongation of such kind of treatment was increased (Figure 4.14(b)). Thus, the combined treatment involving nano reinforcement and both treatments is not so effective in enhancing shear

strength as nano reinforced anodizing process, because electrochemical treatment more specifically focuses on maximizing the shear strength. This type of treatment also showed the mixed failure type (Figure 4.15).

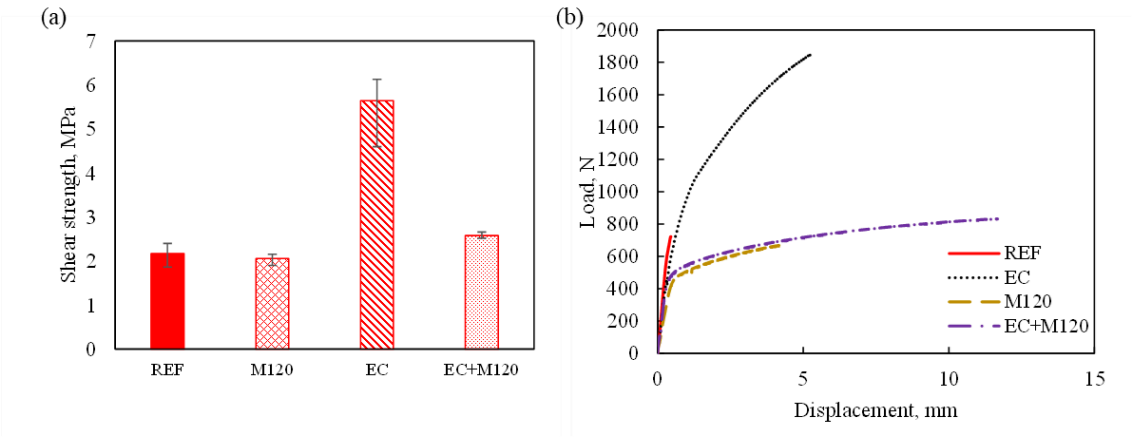

Figure 4.14. Effect of different treatment types on samples with 0.5 wt% α-ZrP: a) Shear strength, b) Load and displacement

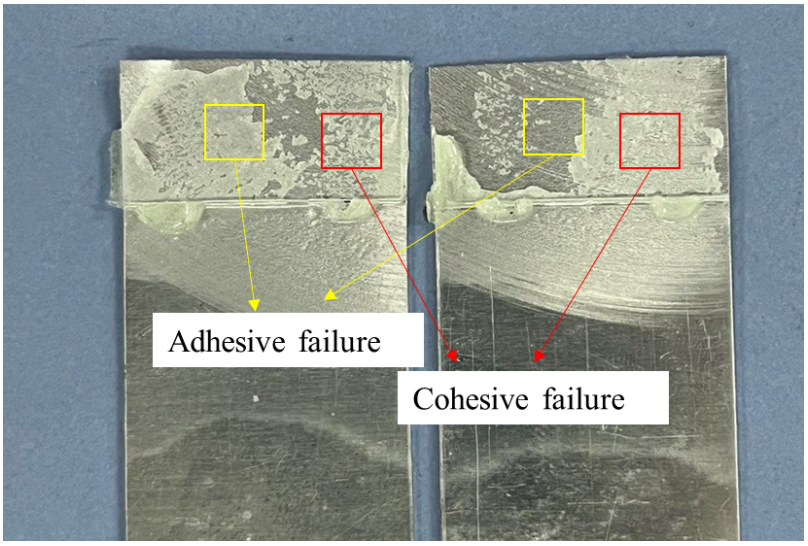

Figure 4.15. The mixed failure of Mechanical with EC (0.5 wt%) sample

4.6 Numerical

According to Figure 4.16, the degradation of the cohesive layer spreads from the edges to the center, which leads to the separation of the laps. This result corresponds to the expected damage distribution in Figure 2.5.

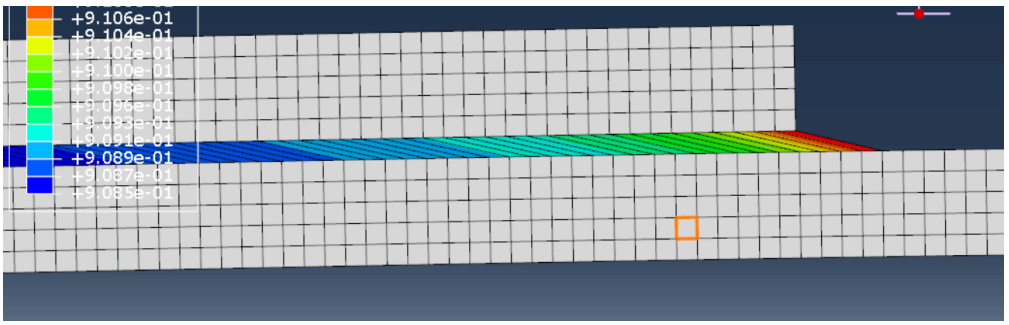

Figure 4.16. Scalar stiffness degradation in a cohesive layer

According to the simulation results shown in Figure 4.17, the largest stress is applied on laps, where edges of the adhesive layer connect laps to each other. It is linked with discontinuity, since change in geometry at the edges creates stress concentrations. Discontinuities are sources of stress intensification. They usually produce peak stresses. If we compare it with Figure 2.4, it can be concluded that this result satisfies the expected one which was based on the reviewed papers with similar topics. Since stress is concentrated near the edges of the adhesive layer, most of the damage is caused there.

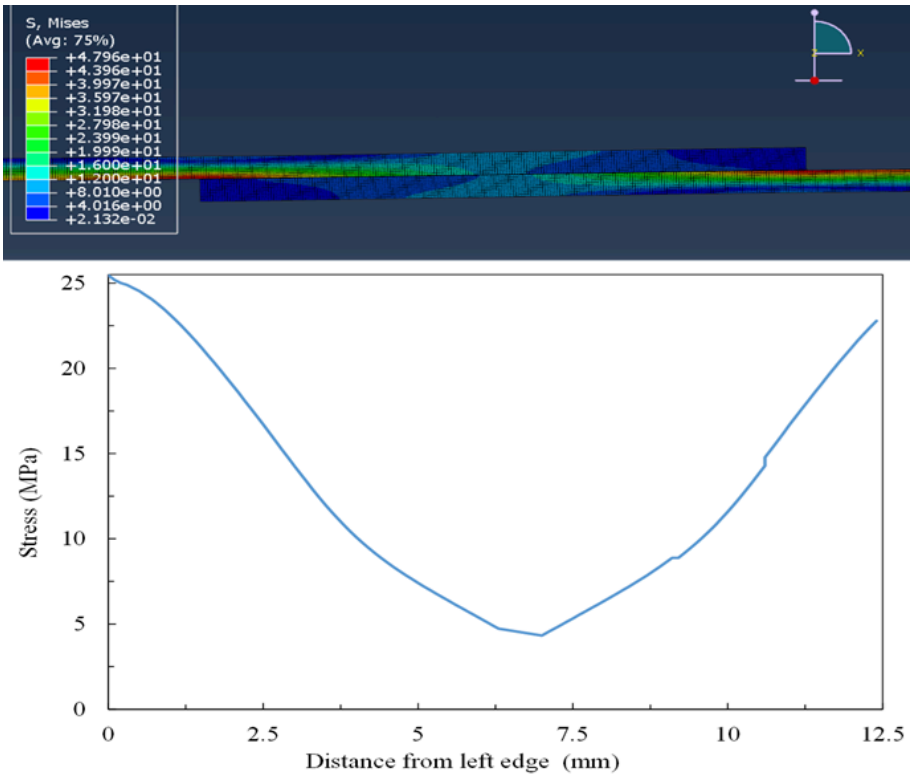

Figure 4.17. Stress distribution along length of adhesive zone of polyethylene with 0 wt% α-ZrP

According to Figure 4.18, it can be noticed that the slope of experimental curve decreases when displacement becomes larger than 0.05 mm. Moreover, the difference in shape between the two curves is probably linked with the meshing of the simulation model. On the other hand, it can be seen that the maximum load (434.3 N) is a little bit larger than the experimental one (393.4 N). The difference in maximum load is about 9.42%. Moreover, the values of experimental and simulated strains at the peak loads are close to each other (0.225 and 0.21 mm respectively). These factors are the most significant ones, which shows reliability of the simulation, while also proving that the experimental part was done correctly.

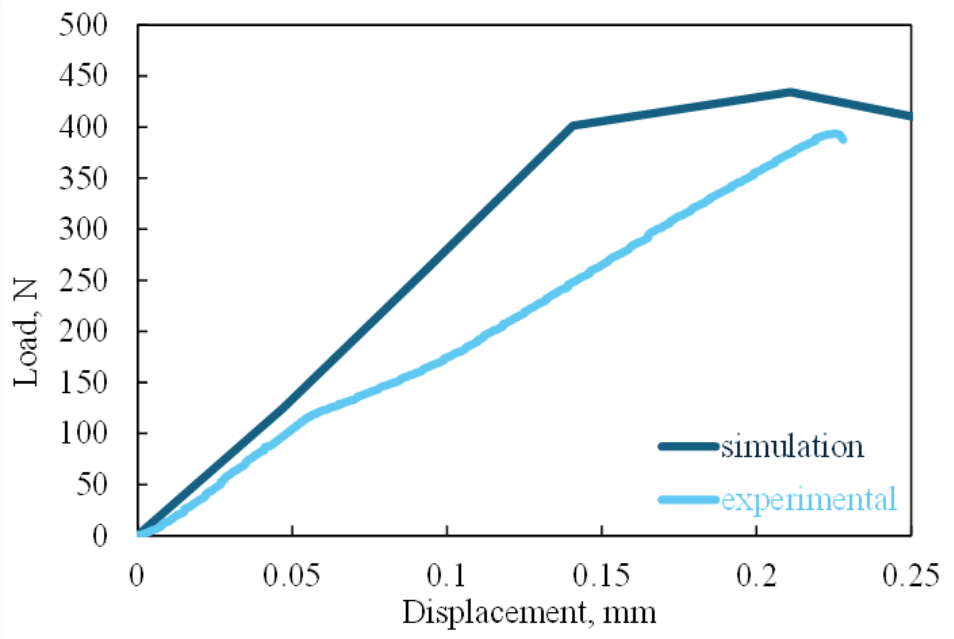

Figure 4.18. Load vs displacement curve of polyethylene with 0 wt% α-ZrP

Chapter 5

Conclusion and Future work

The aim of the research was to implement the nanoparticles in order to reinforce the adhesive layer of the fiber-metal laminates. The commercial polyurethane polymers were made and tested with α-ZrP nanoparticles in a percentage by weight from 0 wt% to 2 wt%. The goal of the numerical part was to validify the experimental data. Simulation was run for polyurethane with 0 wt% of α-ZrP.

- During fabrication of the fiber-metal laminates several hypotheses were tested and proved such that nanoparticles indeed can enhance the strength of the polymer and the best concentration for the pure polymer was found to be 1.0 wt% of α-ZrP and the tensile strength was enhanced 3.5 times compared to the reference sample with no nanoparticles (0 wt%)
- The best concentration for the single lap joints was found to be the polymer of 0.5 wt% of α-ZrP with an increase in shear strength by 91.8%
- Mechanical treatment improved the shear strength of the single lap joints by 35%. However, in combination with nanoparticles, the results were weaker, leading to decrease in the strength. Therefore, it is recommended to use sandpapers with greater intervals between the grit sizes
- Electrochemical treatment also enhanced the load-bearing capabilities of SLJs and combining it with nanoparticles resulted in even higher values, increasing the strength by 174% compared to the mechanical treatment
- Combining nano reinforcement and both treatments also increased the strength by 18.9%, but showed weaker results than for nano reinforced EC treatment
- Results of simulation showed that stress was concentrated on edges of the adhesive layer, which makes the deformation region spread from edges to the center of the cohesive region
- The numerical maximum load of 434.3 N slightly surpasses the experimental value of 393.4 N. The difference in strength between experimental and simulation was less than 9.42%. That proved the reliability of experimental results

By doing the simulation some issues were faced, due to lack of data about material properties in mode I and mode II, which is linked with inability to find those values experimentally. Moreover, since use of α-ZrP nanoparticles as a reinforcing 2D material is an innovative idea, no literature about polyurethane with added α-ZrP was found to get needed coefficients for simulation.

For the future work is planned to conduct experimental tests such as double-cantilever beam (DCB) and end-notched flexure (ENF) ones to get critical strain energy release rate and strength for mode I (G_{IC}) and mode II (G_{IIC}) for samples with different percentages of added α-ZrP nanoparticles.

References

[1] M. Mekhzoum, A. Qaiss, and R. Bouhfid, “Introduction: different types of smart materials and their practical applications,” in *Polymer Nanocomposite-Based Smart Materials*, Woodhead Publishing, 2020, pp. 1–19. doi: 10.1016/B978-0-08-103013-4.00001-7.

[2] J. W. Martin, *Composite materials*. Woodhead Publishing, 2006, pp. 185–215. doi: 10.1533/9781845691608.2.185.

[3] K. Malik *et al.*, “Mechanical property enhancement of graphene-kenaf-epoxy multiphase composites for automotive applications,” *Compos. Part Appl. Sci. Manuf.*, vol. 177, p. 107916, Feb. 2024, doi: 10.1016/j.compositesa.2023.107916.

[4] T. Trzepieciński, S. Mohammed Najm, M. Sbayti, H. Belhadjsalah, M. Szpunar, and H. G. Lemu, “J. Compos. Sci. | Free Full-Text | New Advances and Future Possibilities in Forming Technology of Hybrid Metal–Polymer Composites Used in Aerospace Applications.” Accessed: Apr. 15, 2024. [Online]. Available: https://www.mdpi.com/2504-477X/5/8/217

[5] T. Sinmazçelik, E. Avcu, M. Ö. Bora, and O. Çoban, “A review: Fibre metal laminates, background, bonding types and applied test methods,” *Mater. Des.*, vol. 32, no. 7, pp. 3671–3685, Aug. 2011, doi: 10.1016/j.matdes.2011.03.011.

[6] M. Thirukumaran, I. Siva, J. W. Jappes, and V. Manikandan, “Forming and drilling of fiber metal laminates – A review,” *J. Reinf. Plast. Compos.*, vol. 37, no. 14, pp. 981–990, Jul. 2018, doi: 10.1177/0731684418771194.

[7] S. Wang *et al.*, “Investigation on graphene addition on the quasi-static and dynamic responses of carbon fibre-reinforced metal laminates,” *Thin-Walled Struct.*, vol. 174, p. 109092, May 2022, doi: 10.1016/j.tws.2022.109092.

[8] D. Agrawal, “Evaluation of Surface Treatment for Enhancing Adhesion at the Metal–Composite Interface in Fibre Metal-Laminates - PMC.” Accessed: Apr. 17, 2024. [Online]. Available: https://www.ncbi.nlm.nih.gov/pmc/articles/PMC9458037/

[9] M. V. Ramos-Garcés and J. L. Colón, “Preparation of Zirconium Phosphate Nanomaterials and Their Applications as Inorganic Supports for the Oxygen Evolution Reaction,” *Nanomaterials*, vol. 10, no. 5, p. 822, Apr. 2020, doi: 10.3390/nano10050822.

[10] Q. H. Qin, “1 - Introduction to the composite and its toughening mechanisms,” in *Toughening Mechanisms in Composite Materials*, Q. Qin and J. Ye, Eds., in Woodhead Publishing Series in Composites Science and Engineering. , Woodhead Publishing, 2015, pp. 1–32. doi: 10.1016/B978-1-78242-279-2.00001-9.

[11] H. Li *et al.*, “Reinforcement effects of aluminum–lithium alloy on the mechanical properties of novel fiber metal laminate,” *Compos. Part B Eng.*, vol. 82, pp. 72–77, Dec. 2015, doi: 10.1016/j.compositesb.2015.08.013.

[12] V. V. Antipov, “Efficient aluminum-lithium alloys 1441 and layered hybrid composites based on it,” *Metallurgist*, vol. 56, no. 5, pp. 342–346, Sep. 2012, doi: 10.1007/s11015-012-9581-0.

[13] M. Smolnicki, Sz. Duda, P. Stabla, and T. Osiecki, “Mechanical investigation on interlaminar behaviour of inverse FML using acoustic emission and finite element method,” *Compos. Struct.*, vol. 294, p. 115810, Aug. 2022, doi: 10.1016/j.compstruct.2022.115810.

[14] H. Li, Y. Xu, X. Hua, C. Liu, and J. Tao, “Bending failure mechanism and flexural

properties of GLARE laminates with different stacking sequences," *Compos. Struct.*, vol. 187, pp. 354–363, Mar. 2018, doi: 10.1016/j.compstruct.2017.12.068.
[15] K. Jin, H. Wang, J. Tao, and X. Zhang, "Interface strengthening mechanisms of Ti/CFRP fiber metal laminate after adding MWCNTs to resin matrix," *Compos. Part B Eng.*, vol. 171, pp. 254–263, Aug. 2019, doi: 10.1016/j.compositesb.2019.05.005.
[16] Y. Han, C. Lin, X. Han, Y. Chang, C. Guo, and F. Jiang, "Fabrication, interfacial characterization and mechanical properties of continuous Al2O3 ceramic fiber reinforced Ti/Al3Ti metal-intermetallic laminated (CCFR-MIL) composite," *Mater. Sci. Eng. A*, vol. 688, pp. 338–345, Mar. 2017, doi: 10.1016/j.msea.2017.02.024.
[17] P. Xu, Z. Zhou, T. Liu, and A. Mal, "Determination of geometric role and damage assessment in hybrid fiber metal laminate (FML) joints based on acoustic emission," *Compos. Struct.*, vol. 270, p. 114068, Aug. 2021, doi: 10.1016/j.compstruct.2021.114068.
[18] Y. Guo *et al.*, "Study on formability and failure modes of steel/CFRP based FMLs consisting of carbon fiber reinforced polymer prepreg and steel sheet," *Compos. Struct.*, vol. 281, p. 114980, Feb. 2022, doi: 10.1016/j.compstruct.2021.114980.
[19] X. Zhang *et al.*, "Effect of multi-walled carbon nanotubes addition on the interfacial property of titanium-based fiber metal laminates," *Polym. Compos.*, vol. 39, pp. E1159–E1168, 2018, doi: 10.1002/pc.24670.
[20] S. N. Hosseini Abbandanak, M. Abdollahi Azghan, A. Zamani, M. Fallahnejad, R. Eslami-Farsani, and H. Siadati, "Effect of graphene on the interfacial and mechanical properties of hybrid glass/Kevlar fiber metal laminates," *J. Ind. Text.*, vol. 51, no. 2_suppl, pp. 2576S-2593S, Jun. 2022, doi: 10.1177/1528083720932222.
[21] F. Bahari-Sambran, J. Meuchelboeck, E. Kazemi-Khasragh, R. Eslami-Farsani, and S. Arbab Chirani, "The effect of surface modified nanoclay on the interfacial and mechanical properties of basalt fiber metal laminates," *Thin-Walled Struct.*, vol. 144, p. 106343, Nov. 2019, doi: 10.1016/j.tws.2019.106343.
[22] A. A. Khurram, R. Hussain, H. Afzal, A. Akram, and T. Subhanni, "Carbon nanotubes for enhanced interface of fiber metal laminate," *Int. J. Adhes. Adhes.*, vol. 86, pp. 29–34, Nov. 2018, doi: 10.1016/j.ijadhadh.2018.08.008.
[23] M. Zaczynska and R. J. Mania, "Dynamic stability of thin-walled FML columns including delamination," *Compos. Struct.*, vol. 290, p. 115478, Jun. 2022, doi: 10.1016/j.compstruct.2022.115478.
[24] A. S. Al-Azzawi, L. F. Kawashita, and C. A. Featherston, "Predicting interlaminar damage behaviour of fibre-metal laminates containing adhesive joints under bending loads," *J. Reinf. Plast. Compos.*, vol. 41, no. 5–6, pp. 167–186, Mar. 2022, doi: 10.1177/07316844211051706.
[25] M. Megahed, M. A. Abd El-baky, A. M. Alsaeedy, and A. E. Alshorbagy, "An experimental investigation on the effect of incorporation of different nanofillers on the mechanical characterization of fiber metal laminate," *Compos. Part B Eng.*, vol. 176, p. 107277, Nov. 2019, doi: 10.1016/j.compositesb.2019.107277.
[26] H. Aghamohammadi, R. Eslami-Farsani, and A. Tcharkhtchi, "The effect of multi-walled carbon nanotubes on the mechanical behavior of basalt fibers metal laminates: An experimental study," *Int. J. Adhes. Adhes.*, vol. 98, p. 102538, Apr. 2020, doi: 10.1016/j.ijadhadh.2019.102538.
[27] M. Askin and Y. Turen, "The effect of GNP addition on mechanical and residual stress properties of 2024-T3 aluminum and carbon fiber reinforced FML -

IOPscience.” Accessed: Nov. 26, 2023. [Online]. Available: https://iopscience.iop.org/article/10.1088/2053-1591/ab575b/meta
[28] H. Zarei, T. Brugo, J. Belcari, H. Bisadi, G. Minak, and A. Zucchelli, “Low velocity impact damage assessment of GLARE fiber-metal laminates interleaved by Nylon 6,6 nanofiber mats,” *Compos. Struct.*, vol. 167, pp. 123–131, May 2017, doi: 10.1016/j.compstruct.2017.01.079.
[29] H. Ding, A. Ahmed, K. Shen, and L. Sun, “Assembly of exfoliated α-zirconium phosphate nanosheets: Mechanisms and versatile applications,” *Aggregate*, vol. 3, no. 4, p. e174, 2022, doi: 10.1002/agt2.174.
[30] D. Capitani, M. Casciola, A. Donnadio, and R. Vivani, “High Yield Precipitation of Crystalline α-Zirconium Phosphate from Oxalic Acid Solutions,” *Inorg. Chem.*, vol. 49, no. 20, pp. 9409–9415, Oct. 2010, doi: 10.1021/ic101200f.
[31] Y. He *et al.*, “Combined effect of interfacial modification and α-ZrP reinforcement on the tribological properties of PPS fabric/phenolic composites,” *Colloids Surf. Physicochem. Eng. Asp.*, vol. 648, p. 129118, Sep. 2022, doi: 10.1016/j.colsurfa.2022.129118.
[32] H. Aghamohammadi, S. N. Hosseini Abbandanak, R. Eslami-Farsani, and S. M. H. Siadati, “Effects of various aluminum surface treatments on the basalt fiber metal laminates interlaminar adhesion,” *Int. J. Adhes. Adhes.*, vol. 84, pp. 184–193, Aug. 2018, doi: 10.1016/j.ijadhadh.2018.03.005.
[33] M. Mohamad, H. F. A. Marzuki, E. A. E. Ubaidillah, M. F. Z. Abidin, S. Omar, and I. M. Rozi, “Effect of surface roughness on mechanical properties of aluminium-carbon laminates composites,” *Adv. Mater. Res.*, vol. 879, pp. 51–57, 2014, doi: 10.4028/www.scientific.net/AMR.879.51.
[34] D. J. Arrowsmith and A. W. Clifford, “Morphology of anodic oxide for adhesive bonding of aluminum,” *Int. J. Adhes. Adhes.*, vol. 3, no. 4, pp. 193–196, Oct. 1983, doi: 10.1016/0143-7496(83)90093-3.
[35] H. F. Ahmad Marzuki *et al.*, “Effect of Anodizing on Strength of Carbon-Fibre Aluminium-Laminated Composites,” *Adv. Mater. Res.*, vol. 748, pp. 216–221, Aug. 2013, doi: 10.4028/www.scientific.net/AMR.748.216.
[36] V. Fiore, F. Di Franco, R. Miranda, M. Santamaria, D. Badagliacco, and A. Valenza, “Effects of anodizing surface treatment on the mechanical strength of aluminum alloy 5083 to fibre reinforced composites adhesive joints,” *Int. J. Adhes. Adhes.*, vol. 108, p. 102868, Jul. 2021, doi: 10.1016/j.ijadhadh.2021.102868.
[37] X. Zheng, Z. Zhao, Z. Chu, H. Yin, and W. Wang, “Effect of surface treatment methods on the interfacial behavior of fiber metal laminate based on WE43 magnesium alloy,” *Int. J. Adhes. Adhes.*, vol. 110, p. 102957, Oct. 2021, doi: 10.1016/j.ijadhadh.2021.102957.
[38] Y. Singh, J. Kumar, I. Singh, and P. K. Rakesh, “3 - Joining behavior of natural fiber reinforced polymer composites,” in *Joining Processes for Dissimilar and Advanced Materials*, P. Rakesh and J. P. Davim, Eds., in Woodhead Publishing Reviews: Mechanical Engineering Series. , Woodhead Publishing, 2022, pp. 33–63. doi: 10.1016/B978-0-323-85399-6.00018-7.
[39] S. Bayramoglu, S. Akpinar, and A. Çalık, “Numerical analysis of elasto-plastic adhesively single step lap joints with cohesive zone models and its experimental verification,” *J. Mech. Sci. Technol.*, vol. 35, no. 2, pp. 641–649, Feb. 2021, doi: 10.1007/s12206-021-0124-0.
[40] R. Rodríguez, P. Sollero, M. Bertoni, and E. Albuquerque, *STRESS ANALYSIS AND FAILURE CRITERIA OF ADHESIVE BONDED SINGLE LAP JOINTS*.

2011.
[41] T. M. S. Faneco, R. Campilho, and R. Lopes, “Strength and Fracture Characterization of a Novel Polyurethane Adhesive for the Automotive Industry,” *J. Test. Eval.*, vol. 45, pp. 398–407, Mar. 2017, doi: 10.1520/JTE20150335.
[42] K. Malik, F. Ahmad, N. A. Yunus, E. Gunister, and C. A. Shahed, “Mechanical Investigation of Kenaf/Carbon Hybrid Composites for Building and Construction Applications,” *J. Compos. Constr.*, vol. 28, no. 1, p. 04023066, Feb. 2024, doi: 10.1061/JCCOF2.CCENG-4258.
[43] T. Chengguang, Z. Xiaosheng, X. Hong, and D. Jinxiang, “Synthesis and Tribological Properties of Sodium-Ion-Exchanged α-Zirconium Phosphate.” Accessed: Apr. 21, 2024. [Online]. Available: http://www.chinarefining.com/EN/abstract/abstract764.shtml
[44] Y. Zhou *et al.*, “Gold nanoparticles immobilized on single-layer α-zirconium phosphate nanosheets as a highly effective heterogeneous catalyst,” *Adv. Compos. Hybrid Mater.*, vol. 2, no. 3, pp. 520–529, Sep. 2019, doi: 10.1007/s42114-019-00091-x.
[45] M. B. Kale, N. Divakaran, S. Mubarak, D. Dhamodharan, T. Senthil, and L. Wu, “Waterborne polyurethane nanocomposite reinforced with amine intercalated α-zirconium phosphate - Study of thermal and mechanical properties,” *Polymer*, vol. 186, p. 122008, Jan. 2020, doi: 10.1016/j.polymer.2019.122008.
[46] P. K. Mallick, *Fiber-Reinforced Composites: Materials, Manufacturing, and Design, Third Edition*, 3rd ed. Boca Raton: CRC Press, 2007. doi: 10.1201/9781420005981.
[47] Y. Pan, G. Wu, Z. Huang, M. Li, S. Ji, and Z. Zhang, “Effect of surface roughness on interlaminar peel and shear strength of CFRP/Mg laminates,” *Int. J. Adhes. Adhes.*, vol. 79, pp. 1–7, Dec. 2017, doi: 10.1016/j.ijadhadh.2017.08.004.